Biodiversity and Climate Change Project - BIOCLIME

Survey of biomass, carbon stocks, biodiversity, and assessment of the historic fire regime for integration into a forest monitoring system in the Districts Musi Rawas, Musi Rawas Utara, Musi Banyuasin and Banyuasin, South Sumatra, Indonesia

Project number: 12.9013.9-001.00

Work Package 4
Historic fire regime

Final Report

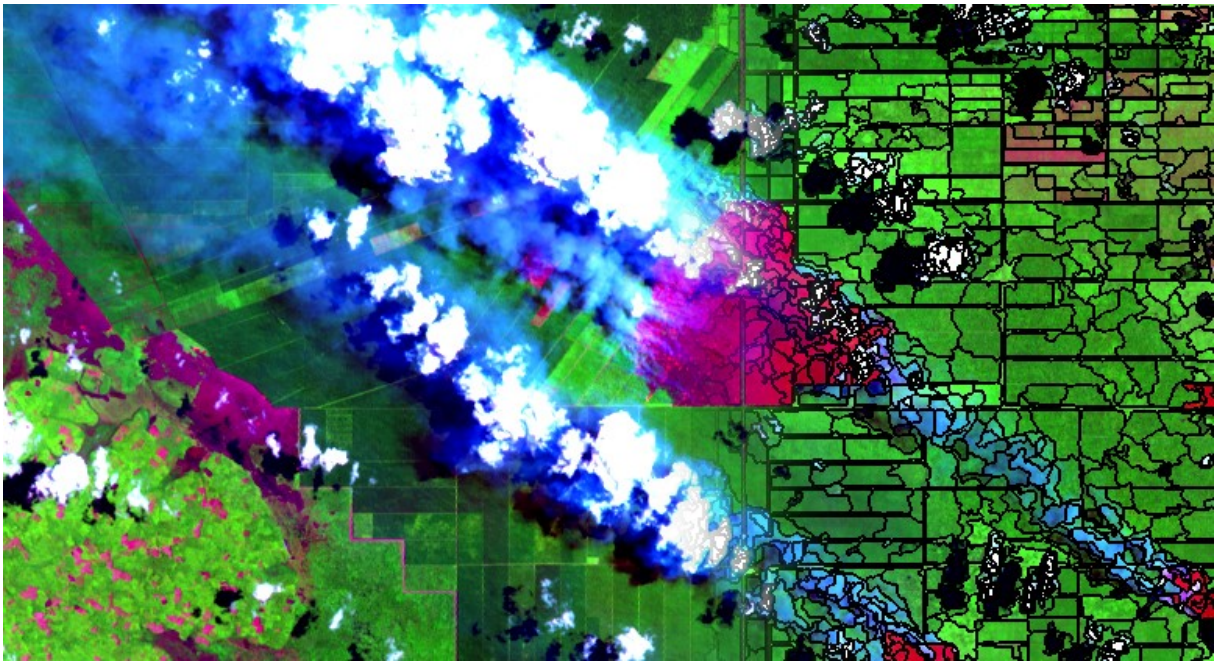

Prepared by:

Dr. Uwe Ballhorn, Matthias Stängel, Peter Navratil, Dr. Sandra Lohberger, Werner Wiedemann, Prof Dr. Florian Siegert

RSS – Remote Sensing Solutions GmbH

Isarstraße 3
82065 Baierbrunn
Germany
Phone: +49 89 48 95 47 66
Fax: +49 89 48 95 47 67
Email: ballhorn@rssgmbh.de

November 2016

Table of Content

1. Introduction

With the Biodiversity and Climate Change Project (BIOCLIME), Germany supports Indonesia's efforts to reduce greenhouse gas emissions from the forestry sector, to conserve forest biodiversity of High Value Forest Ecosystems, maintain their Carbon stock storage capacities and to implement sustainable forest management for the benefit of the people. Germany's immediate contribution will focus on supporting the Province of South Sumatra to develop and implement a conservation and management concept to lower emissions from its forests, contributing to the GHG emission reduction goal Indonesia has committed itself until 2020.

One of the important steps to improve land-use planning, forest management and protection of nature is to base the planning and management of natural resources on accurate, reliable and consistent geographic information. In order to generate and analyze this information, a multi-purpose monitoring system is required.

This system will provide a variety of information layers of different temporal and geographic scales:

- Information on actual land-use and the dynamics of land-use changes during the past decades is considered a key component of such a system. For South Sumatra, this data is already available from a previous assessment by the World Agroforestry Center (ICRAF).
- Accurate current information on forest types and forest status, in particular in terms of aboveground biomass, carbon stock and biodiversity, derived from a combination of remote sensing and field techniques.
- Accurate information of the historic fire regime in the study area. Fire is considered one of the key drivers shaping the landscape and influencing land cover change, biodiversity and carbon stocks. This information must be derived from historic satellite imagery.
- Indicators for biodiversity in different forest ecosystems and degradation stages.

The objective of the work conducted by Remote Sensing Solutions GmbH (RSS) was to support the goals of the BIOCLIME project by providing the required information on land use dynamics, forest types and status, biomass and biodiversity and the historic fire regime. The conducted work is based on a wide variety of remote sensing systems and analysis techniques, which were jointly implemented within the project, in order to produce a reliable information base able to fulfil the project's and the partners' requirements on the multi-purpose monitoring system.

This report presents the results of Work Package 4 (WP 4): Historic fire regime.

The key objective of this work package was the generation of burned area maps for different years based on optical satellite data. The years for classification were selected based on the numbers of hotspots (MODIS) per year and precipitation distributions. Only the burned areas for severe fire years were classified (1997, 1999, 2002, 2004, 2006, 2009, 2011, 2012, 2014 and 2015). Historic satellite data (Landsat-5, Landsat-7 and Landsat-8) was utilized from the period 1997 onwards to assess the historic fire regime. Burned areas were classified based on the combination of two methodologies to increase accuracy. The result of the classification is a yearly map of burned areas within the boundaries of the BIOCLIME study area. Based on these maps a fire frequency map was derived in order to locate areas of higher and lower fire frequency. Based on these annual burned areas emissions were calculated to assess the amount of carbon emitted, from the vegetation cover and the peat soil. The results are annual and total emissions from aboveground biomass, peat burning within the BIOCLIME study area.

The approach chosen to assess the historic fire regime is transferrable to other optical satellite sensors. The workflow is shown in Figure 1.

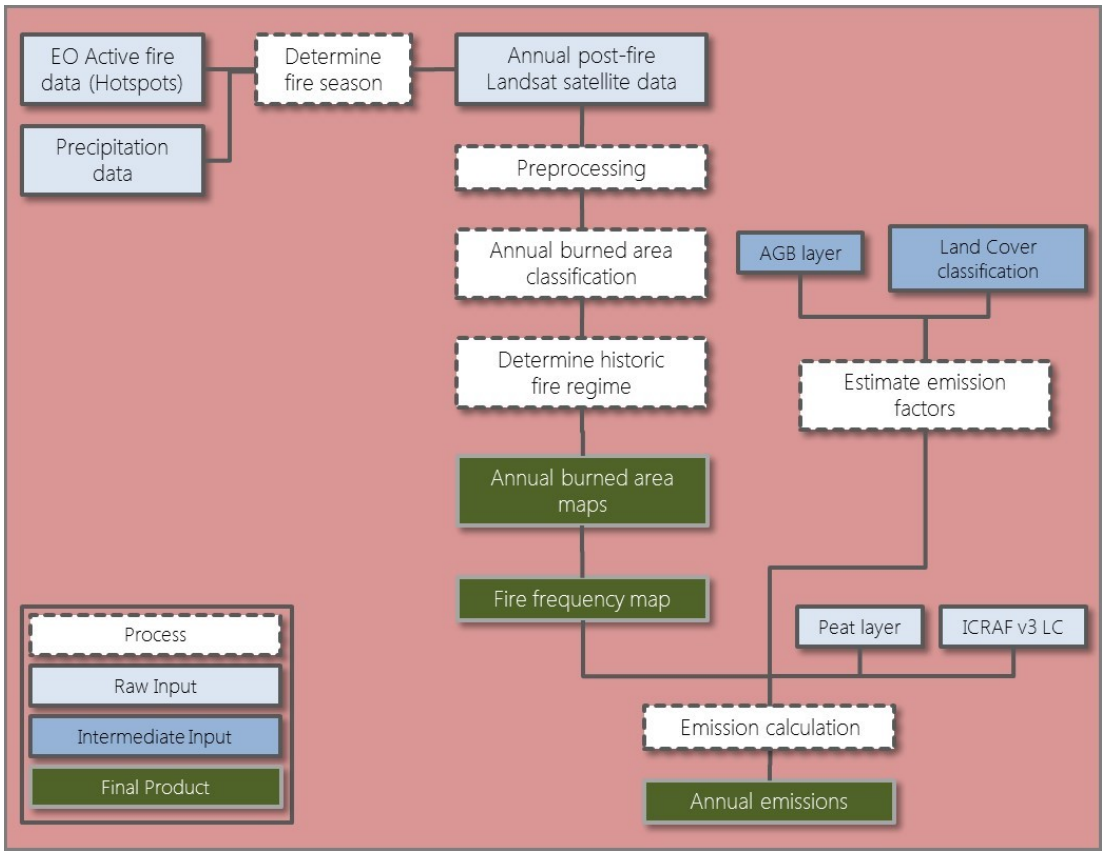

Figure 1: Workflow of the historic fire regime analysis

2. Methodology

2.1 Selection of annual mid resolution images for the years 1990 – 2014

In a first step, the fire season of each year was analyzed on the basis of monthly precipitation and MODIS active fire hotspot data. The latest MODIS Collection 6 hotspot data was provided by the University of Maryland's Fire Information for Resource Management System (FIRMS) as point shapefiles for the time period 2000 onwards. Each hotspot / active fire detection represents the center of a 1 km^2 pixel flagged as containing at least one active fire. The pixel center, and the derived shapefile point location, is not necessarily the real location of the active fire event due to the coarse resolution of the data. The fire season of the pre-MODIS era (before the year 2000) was investigated based on active fire data from the Forest Fire Prevention and Control Project of the European Union and the South Sumatra Forest Fire Management Project (SSFFMP). In addition, the Oceanic Niño Index (available at: http://www.cpc.ncep.noaa.gov/products/analysis_monitoring/ensostuff/ensoyears.shtml), indicating El Niño years with higher fire occurrence, was additionally implemented as indicator for fire seasons with high fire probability. Figure 2 shows an example of a fire season analysis based on precipitation and active fire data.

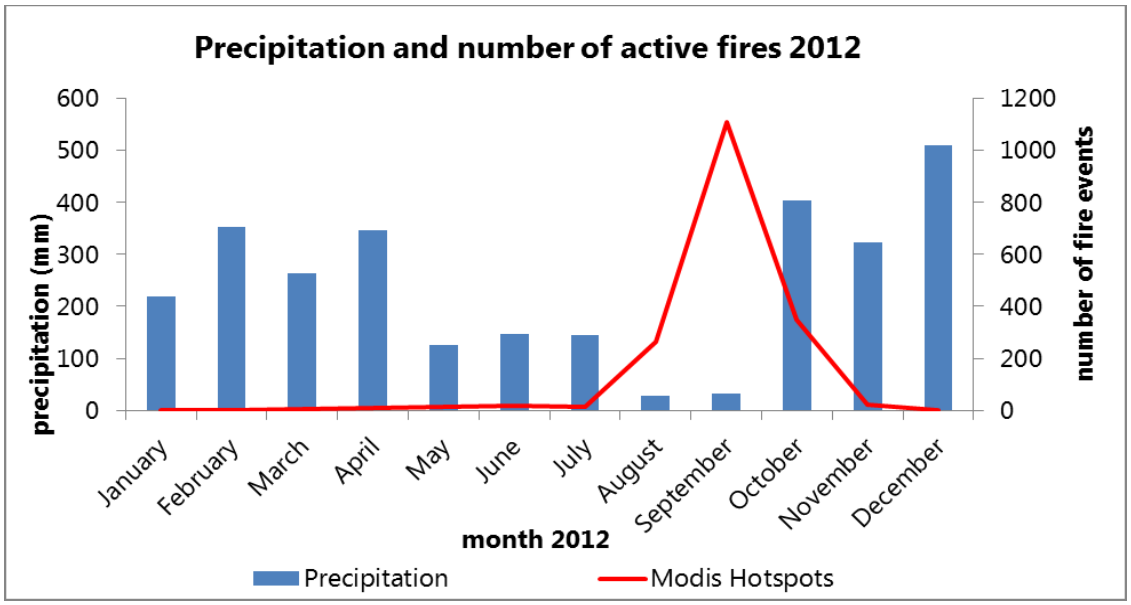

Figure 2: Example of a fire season analysis for a given year based on precipitation data and MODIS active fire data.

Available mid-resolution multispectral imagery was selected from fire season start to approximately two months after fire season end. Landsat-5, Landsat-7 or Landsat-8 images were used for the assessment of the annual burned area. Due to the fast regrowth of vegetation scenes acquired during or shortly after the fire events (mostly during August to October) detect burn scars with higher confidence than scenes acquired outside this period. If no or not enough images were available during or shortly after the fire season (cloud or haze cover), images acquired before the next fire season of the following year were considered. In total, five Landsat tiles are necessary to cover the four districts of the BIOCLIME project area (Figure 3).

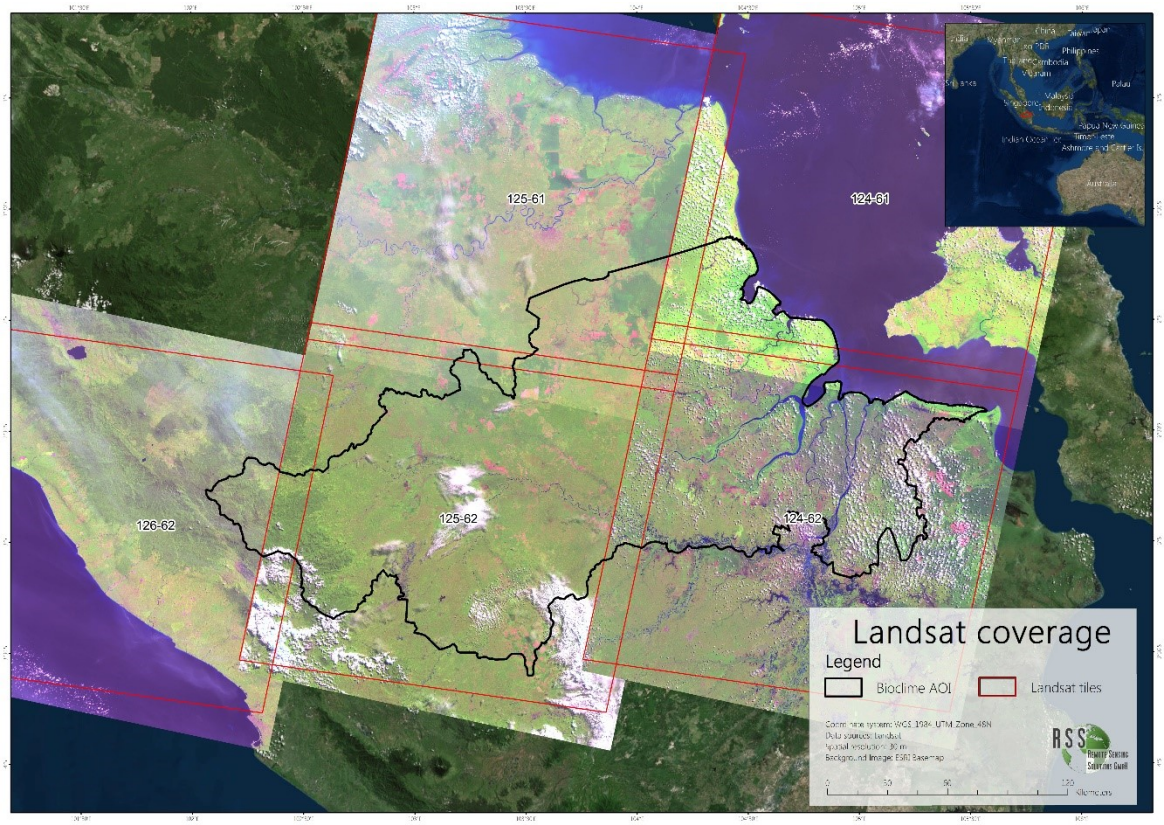

Figure 3: Five Landsat tiles are needed to cover the BIOCLIME project area.

Figure 4 displays the number of MODIS hotspots within the BIOCLIME project area, the years selected for burn area mapping and the number of Landsat scenes considered for the mapping years.

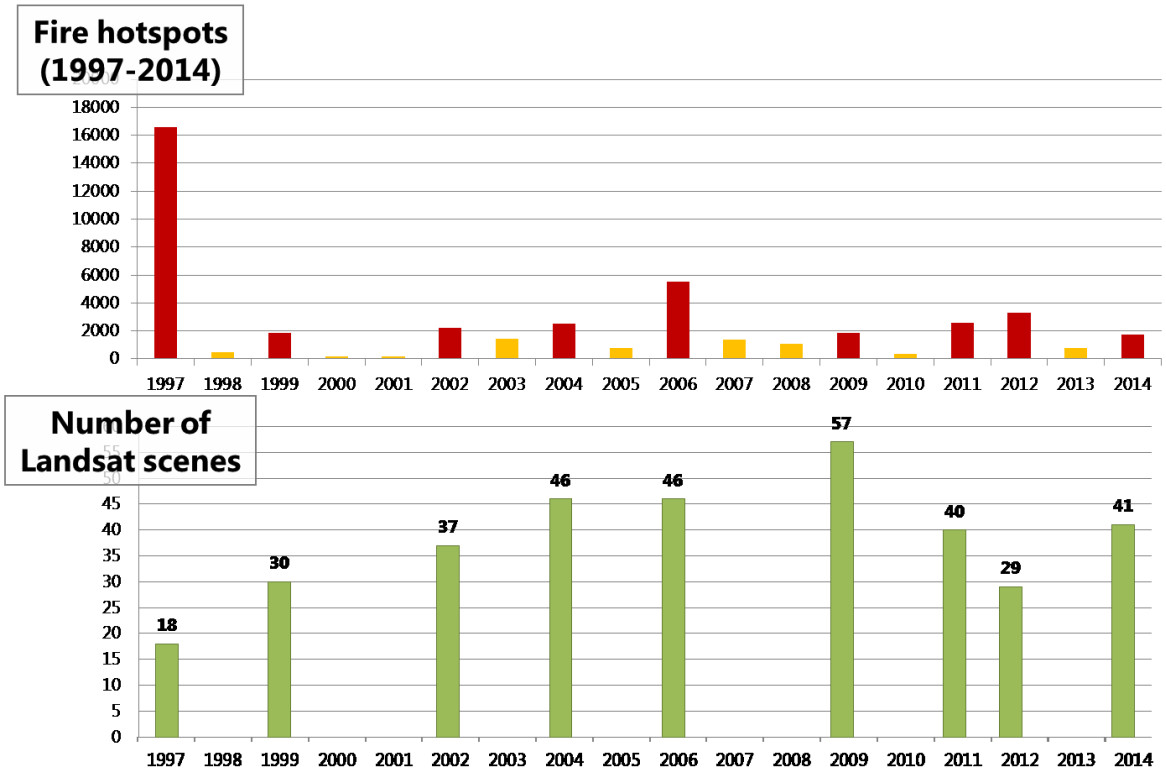

Figure 4: The upper diagram shows the number of MODIS hotspots within the BIOCLIME project area from 1997 to 2014. Red bars indicate the years selected for mapping, yellow bars indicate the years not mapped. The lower diagram depicts the number of considered Landsat scenes for the years mapped.

DATA LIMITATIONS:

The limitations of the historic Landsat imagery used for burn scar detection are given by the technical structure of the instrument itself and the environmental conditions during the acquisition. The technical features of the used satellites sensors are shown in Table 1, Table 2 and Table 3.

Table 1: Technical features of the Landsat 5 sensor (Thematic Mapper (TM)

	Bands	Wavelength (micrometers)	Resolution (meters)
Landsat 5 (8bit) Thematic Mapper (TM)	Band 1	0.45-0.52	30
	Band 2	0.52-0.60	30
	Band 3	0.63-0.69	30
	Band 4	0.76-0.90	30
	Band 5	1.55-1.75	30
	Band 6	10.40-12.50	120* (30)
	Band 7	2.08-2.35	30

Table 2: Technical features of the Landsat 7 sensor (Enhanced Thematic Mapper plus (ETM+)

	Bands	Wavelength (micrometers)	Resolution (meters)
Landsat 7 (8bit) Enhanced Thematic Mapper Plus (ETM+)	Band 1	0.45-0.52	30
	Band 2	0.52-0.60	30
	Band 3	0.63-0.69	30
	Band 4	0.77-0.90	30
	Band 5	1.55-1.75	30
	Band 6	10.40-12.50	60 * (30)
	Band 7	2.08-2.35	30
	Band 8	0.52-0.90	15

Table 3: Technical features of the Landsat 8 sensor (Operational Land Imager (OLI)

	Bands	Wavelength (micrometers)	Resolution (meters)
Landsat 8 (12bit) Operational Land Imager (OLI)	Band 1 - Coastal aerosol	0.43 - 0.45	30
	Band 2 - Blue	0.45 - 0.51	30
	Band 3 - Green	0.53 - 0.59	30
	Band 4 - Red	0.64 - 0.67	30
	Band 5 - Near Infrared (NIR)	0.85 - 0.88	30
	Band 6 - SWIR 1	1.57 - 1.65	30
	Band 7 - SWIR 2	2.11 - 2.29	30
	Band 8 - Panchromatic	0.50 - 0.68	15
	Band 9 - Cirrus	1.36 - 1.38	30
	Band 10 - Thermal Infrared (TIRS) 1	10.60 - 11.19	100 * (30)
	Band 11 - Thermal Infrared (TIRS) 2	11.50 - 12.51	100 * (30)

The spatial resolution of the optical bands and the SWIR (short wave infrared) bands used for classification is 30 meters.

The smallest feature that can be mapped is equal to one pixel (30 m x 30 m for Landsat data used in study). However, it is agreed upon that the smallest observable feature that can be reliably identified needs to consist of more than one contiguous pixels. The reason is that a feature with a size of only one pixel will almost never fall entirely within one pixel, but will instead be split across up to four pixels. Therefore, the feature's reflectance would make up only a fraction of those pixels and thus could not be reliably classified. In order to avoid this effect, a Minimum Mapping Unit (MMU) of 0.5 ha was introduced, representing the smallest possible unit to map.

Furthermore, on May 31, 2003, the Scan Line Corrector (SLC), which compensates for the forward motion of Landsat 7, failed and since leads to stripes in the data without information (see Figure 5).

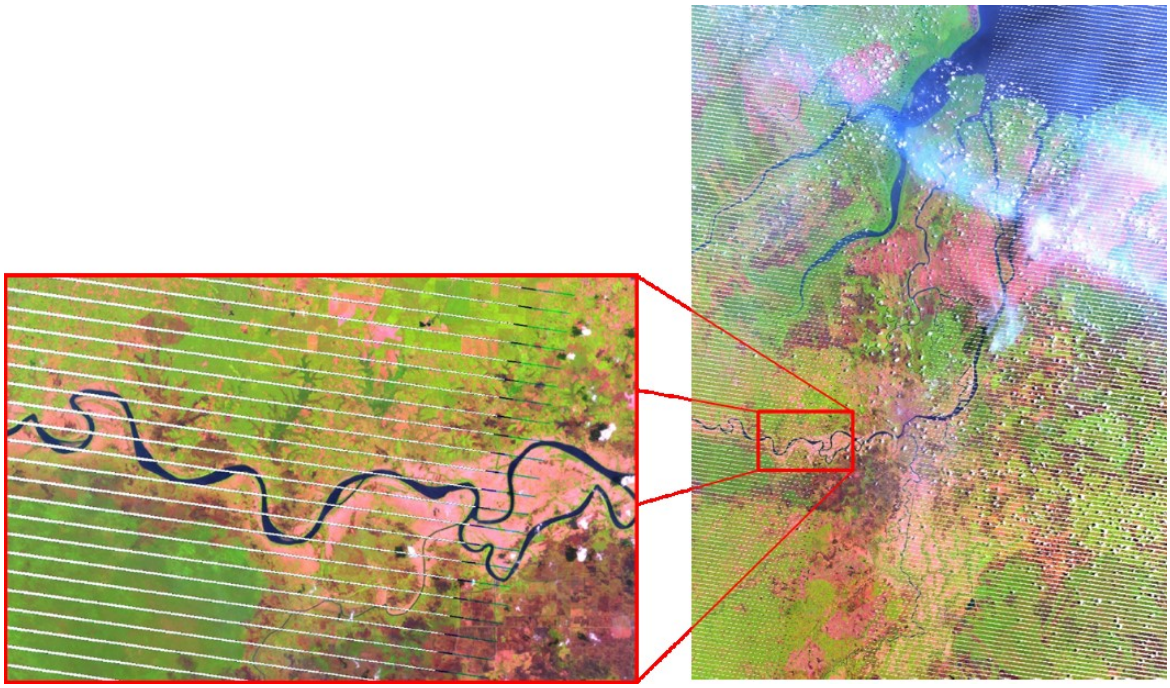

Figure 5: Landsat 7 SLC-off mode, data stripes.

A final constrain concerns the dependency of optical sensors on the atmospheric conditions. Clouds, haze and smoke hamper the opportunity to map burned areas, simply because the burned areas cannot be seen. These limitations were diminished using numerous overlapping scenes to be able to classify as many burned areas as possible.

2.2 Preprocessing: Radiometric and atmospheric correction

The pre-processing for Landsat data consisted of the removal of atmospheric distortions (scattering, illumination effects, adjacency effects), induced by water vapor and aerosols in the atmosphere, seasonally different illumination angles, etc. An atmospheric correction was applied to each image using the software ATCOR (Richter and Schläpfer 2014). This pre-processing step leads to a calibration of the data into an estimation of the surface reflectance without atmospheric distortion effects including topographic normalization. This calibration method facilitates a better scene-to-scene comparability of the radiometric measurements, which is a necessary precondition for the semi-automatic segment-based rule-set classification method applied in this study and the proposed monitoring system.

2.3 Image segmentation

The satellite images were then used as input for burned area classification using an object-based image analysis approach. The first step of the object-based approach is to generate so called "image-objects" which combines spatially adjacent and spectrally similar groups of pixels, rather than individual pixels of the image (pixel-based approach).

Traditional pixel-based classification uses multi-spectral classification techniques that assign a pixel to a class by considering the spectral similarities with the class or with other classes. The resulting thematic classifications are often incomplete and non-homogeneous, in particular when being applied to high resolution satellite data and when mapping spectrally heterogeneous classes such as forest. The received

signal frequency does not clearly indicate the membership to a land cover class, e.g. due to atmospheric scattering, mixed pixels, or the heterogeneity of natural land cover.

Improving the spatial resolution of remote sensing systems often results in increased complexity of the data. The representation of real world objects in the feature space is characterized by high variance of pixel values, hence statistical classification routines based on the spectral dimensions are limited and a greater emphasis must be placed on exploiting spatial and contextual attributes (Matsuyama 1987, Guindon 1997, 2000). To enhance classification, the use of spatial information inherent in such data was proposed and studied by many researchers (Atkinson and Lewis 2000).

Many approaches make use of the spatial dependence of adjacent pixels. Approved routines are the inclusion of texture information, the analysis of the (semi-)variogram, or region growing algorithms that evaluate the spectral resemblance of proximate pixels (Woodcock *et al.* 1988, Hay *et al.* 1996, Kartikeyan *et al.* 1998). In this context, the use of object-oriented classification methods on remote sensing data has gained immense popularity, and the idea behind it was subject to numerous investigations since the 1970's (Kettig and Landgrebe 1976, Haralick and Joo 1986, Kartikeyan *et al.* 1995).

2.4 Mapping annual burned areas: spatial extent and fire severity

Burned areas were classified based on burn ratios (BR) of bands $b_{0.84\mu m}$, $b_{2.22\mu m}$, and $b_{11.45\mu m}$:

$$BR1 = (b_{0.84\mu m} - b_{11.45\mu m}) / (b_{0.84\mu m} + b_{11.45\mu m}) \quad \text{(eq. 1)}$$

where $b_{0.84\mu m}$ is the reflectance value of Near Infrared (0.76-0.90 µm) and $b_{11.45\mu m}$ is the reflectance value of Thermal Infrared (10.4-12.5µm).

$$BR2 = (b_{0.84\mu m} - b_{2.22\mu m}) / (b_{0.84\mu m} + b_{11.45\mu m}) \quad \text{(eq. 2)}$$

where $b_{0.84\mu m}$ is the reflectance value of Near Infrared (0.76-0.90 µm), $b_{2.22\mu m}$ is the reflectance value of Mid-Infrared (2.08-2.35 µm) and $b_{11.45\mu m}$ is the reflectance value of Thermal Infrared (10.4-12.5µm).

$$NBR = (b_{0.84\mu m} - b_{2.22\mu m})/(b_{0.84\mu m} + b_{2.22\mu m}) \quad \text{(eq. 3)}$$

where $b_{0.84\mu m}$ is the reflectance value of Near Infrared (0.76-0.90 µm) and $b_{2.22\mu m}$ is the reflectance value of Mid-Infrared (2.08-2.35 µm).

The Normalized Burn Ratio (NBR) was used to assess the fire intensity. The ratios BR1 and BR2 have already been successfully applied for burned area mapping in the province Riau, Sumatra (Baier 2014).

Additionally, the normalized difference vegetation index (NDVI) was calculated to improve the detection of clouds, water and burned areas.

$$NDVI = (b_{0.84\mu m} - b_{0.66\mu m})/(b_{0.84\mu m} + b_{0.66\mu m}) \quad \text{(eq. 4)}$$

where $b_{0.84\mu m}$ is the reflectance value of Near Infrared (0.76-0.90 µm) and $b_{0.66\ \mu m}$ is the reflectance value of red (0.64 - 0.67µm).

Burned area classification was conducted on 15 Landsat images to find a fixed threshold (mean threshold value of the 15 Landsat images) which then was applied to all Landsat scenes. Thresholds were determined for BR1, BR2 and NBR. Previous work has shown that BR1 and BR2 are more useful than NBR for classifying burned areas as the influence of haze or shadow is minimized. Figure 6 shows an example of a Landsat 8 subset and the overall workflow from the initial image to the final classification. Each classification result was manually post-processed to eliminate misclassifications. Burned areas were exported as a shapefile and merged for each fire year.

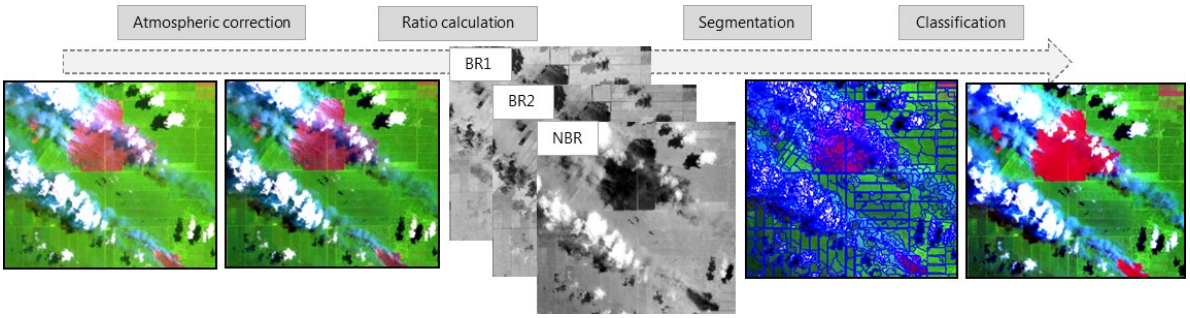

Figure 6: Processing steps from atmospheric correction of the Landsat data to the segmentation and finally the classification.

2.5 Mapping approaches

We combined two object-based approaches to overcome particular limitations of each single approach. Combining both outputs lead to the best results of burned area classification. After the automatic classification manual revision was necessary especially in areas with a lot of smoke and/or haze.

A water and cloud-mask was applied to all images before processing based on the normalized difference water index (NDWI) and Cloud-Index (based on the Quality Assessment band provided by USGS) in order to avoid misclassifications in water and cloud/cloud shadow areas.

$$NDWI = (b_{0.84\mu m} - b_{1.57\mu m})/(b_{0.84\mu m} + b_{1.57\mu m}) \quad \text{(eq. 5)}$$

Where $b_{0.84\mu m}$ is the reflectance value of Near Infrared (0.76 - 0.90 µm) and $b_{1.57\mu m}$ is the reflectance value of Short Wave Infrared (1.57 – 1.65µm).

Figure 7 depicts graphically the two approaches and their combination.

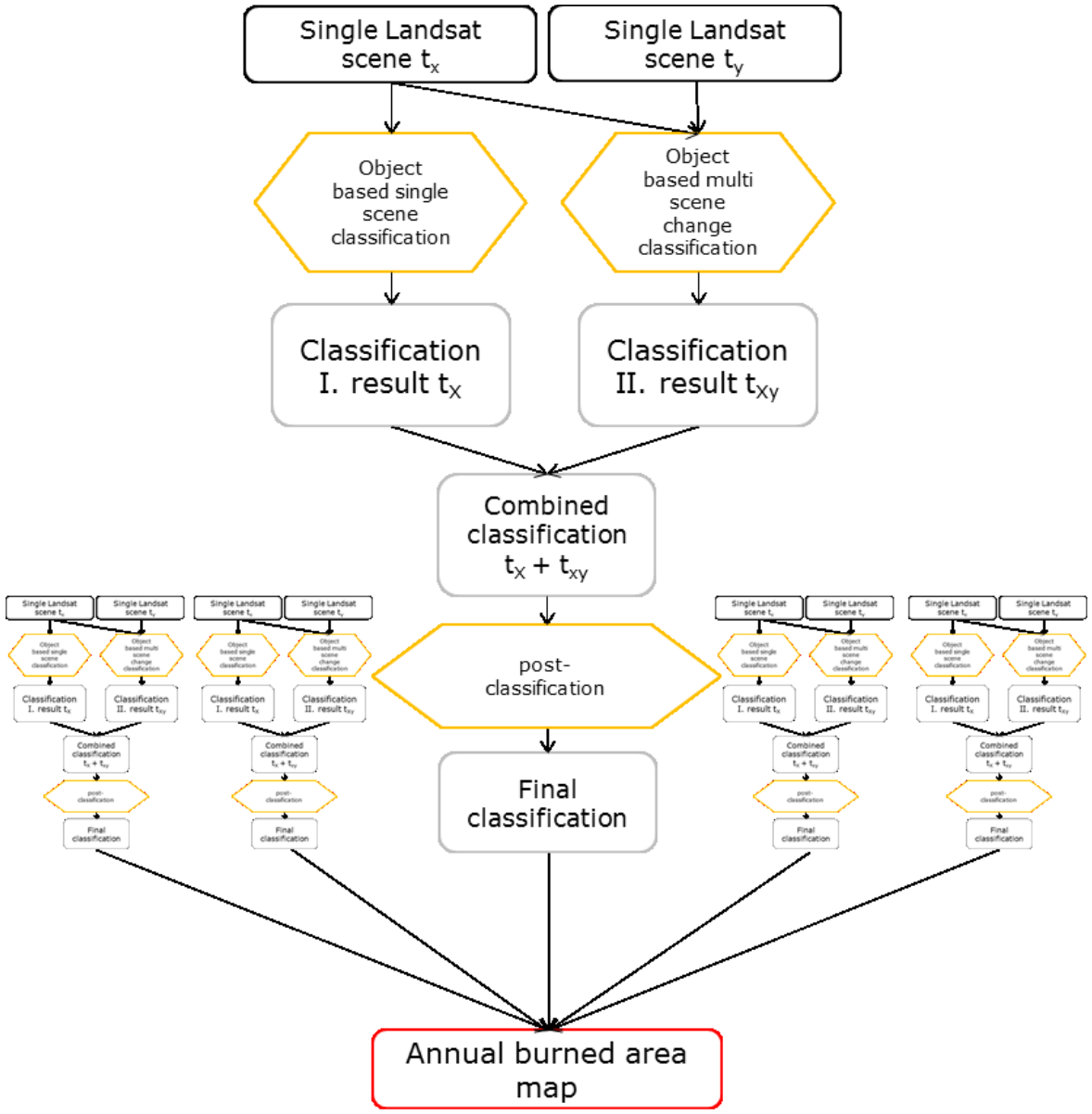

Figure 7: This figure represents both burned are classification workflows and their fusion.

The following three paragraphs will explain the difference between the two approaches, their strength and limitations as well as the final combination of both.

1.1.1 Approach 1 - Object based classification based on single scene

In the single scene approach, burned areas were classified based on one Landsat scene utilizing the derived burn ratios described above. The settings for segmentation and classification enable the detection of small scale burned areas (little agricultural fields) to large scale forest fires.

Thresholds for classifying burned areas were defined by a variable approach based on Landsat image statistics. Fixed thresholds were used for all Landsat scenes, whereas they had to be adjusted for Landsat 8 and Landsat 5/7 due to slightly different wavelengths characteristics. As a last step, the MMU was applied and objects were smoothened.

LIMITATIONS:

The main limitation of the single scene approach is the detection of burned areas in areas with haze. Even though the scenes were atmospherically corrected, the influence of thick haze and/or smoke cannot fully be diminished. Having numerous scenes with haze and or smoke (fire season) lead to the idea of combining this approach with a multi-temporal approach to overcome this limitation (see approach 2).

1.1.2 Approach 2 - Object based multi scene change detection (t1 – t2)

The multi scene approach is based on images with a maximum sensing difference of 32 days which were stacked and segmented based on the multiple spectral bands and the derived Indices (based on an approach by Melchiori *et al.* 2014).

Burn areas were classified by the mean spectral values of an object for the change rate (CR) and the difference (D) CRNDVI, CRNBR, DNBR and NBR. Different thresholds (t) were used for Landsat 8 and Landsat 5/7.

$$crndvi = \frac{ndvi(t1) - ndvi(t2)}{abs(ndvi(t1))} \quad \text{(eq. 6)}$$

$$crnbr = \frac{nbr(t1) - nbr(t2)}{abs(nbr(t1))} \quad \text{(eq. 7)}$$

$$dnbr = nbr(t1) - nbr(t2) \quad \text{(eq. 8)}$$

$$Burnmask = (crnbr \geq Tcnbr) * (crndvi \geq Tcrndvi) * (dnbr > Tdnbr) \quad \text{(eq. 9)}$$

LIMITATIONS:

The main limitation of this approach is the frequent cloud cover in the tropics. Having a cloud in one of the compared scenes hampers the detection of burned areas (see Figure 8). Therefore, both scenes have to be cloud free for classification. However, this approach is superior to approach 1 in areas covered by haze. Another effect that was detected was the classification of bare areas in oil palm plantations which were classified as burned area.

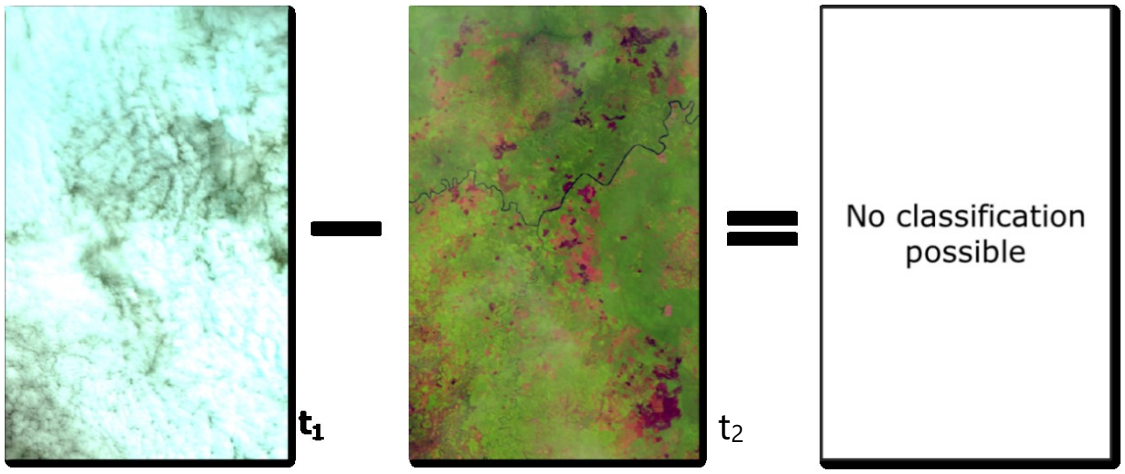

Figure 8: This figure depicts the limitations of the multi scene approach. Clouds in one of the time steps prevent a classification in the cloud free time step.

1.1.3 Combining Approach 1 & Approach 2

The final derived classification is a combination of these two approaches to grant high accuracy and diminish false positives. The aforementioned limitations of both approaches are reduced via the combination of both approaches (see Figure 7). Additionally, the selection of all available Landsat scenes (instead of one cloud free single scene) for classification increased the accuracy. Figure 9 displays a comparison of single scene and multi scene approach for burned area detection.

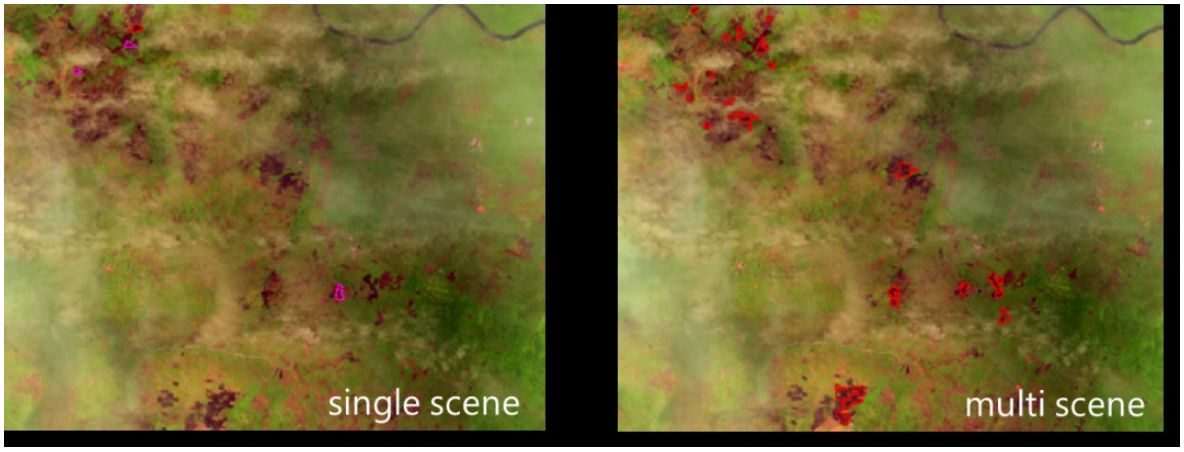

Figure 9: Comparison of single scene and multi scene approach for burned area detection.

2.6 Pre-fire vegetation, area burned and fire frequency

The historic fire regime was analyzed in terms of pre-fire vegetation, fire frequency, and area burned. Fire frequency was evaluated by cumulative merging and intersection of the annual burned areas (see Figure 21). The land cover classification produced by ICRAF for the years 1990, 2000, 2005, 2010 and 2014 (see Work Package 1 (WP 1) was used in order to assess pre-fire land cover class. This helps the identification of the drivers of deforestation. Furthermore, this allows an estimation of the carbon emissions released by fire in South Sumatra since 1990.

Finally, a shapefile was generated containing the following attributes: fire frequency, year of fire(s), pre-fire land cover class and spatial extent (area).

2.7 Accuracy assessment

At the time this report was compiled, no historic reference data was available on burned areas. Therefore, an accuracy assessment could not be conducted.

2.8 Emissions calculation

To calculate the emissions by the fires for each year, the aboveground emissions and peat emissions were calculated. Summing these products up leads to total emissions for each single mapped year. We used the stratify & multiply approach to calculate carbon stock maps from the land cover classifications of Work Package 1 (WP 1) in combination with the local aboveground biomass values derived in Work Package 3 (WP 3), and intersected those carbon stock maps with the fire frequency map for the calculation of the emissions. Emissions are reported in tons of carbon (t C).

Using the stratify & multiply approach for emission calculation first a stratification needs to be applied. We used the ICRAF land cover classification v3 product. This dataset then is intersected with the burned area product of each single year mapped. Each stratum (in our case each land cover class) is attributed with an emission factor (aboveground biomass value) which was derived in WP 3 by using the LiDAR based aboveground biomass (AGB) model and the high spatial resolution land cover maps from Work Package 2 (WP 2). This increases the accuracy of the emissions drastically because the local variations of land cover and biomass directly feed into the emission calculations. To calculate the carbon content of a certain stratum, the biomass is simply divided by 2 (i.e. a carbon content of 0.5 is assumed). By multiplying the burned area with the carbon stock the carbon emissions from burning biomass are calculated.

In addition, the carbon emissions from peat burning were calculated. Peat stores huge amount of carbon and therefore leads to huge emissions when ignited. To calculate these emissions, we used the approach by Konecny *et al.* (2016), which discriminates between first, second and or more fires with regard to the peat burn depth, and therefore the amount of carbon which is released.

To generate the peat emissions the land cover, burned area and peat layers (Peatland distribution for 2016 created by Ministry of Environment and Forestry (MoEF) (see Figure 10)) were intersected. Similar to the emission estimation from AGB, the pre-fire land cover is taken into consideration.

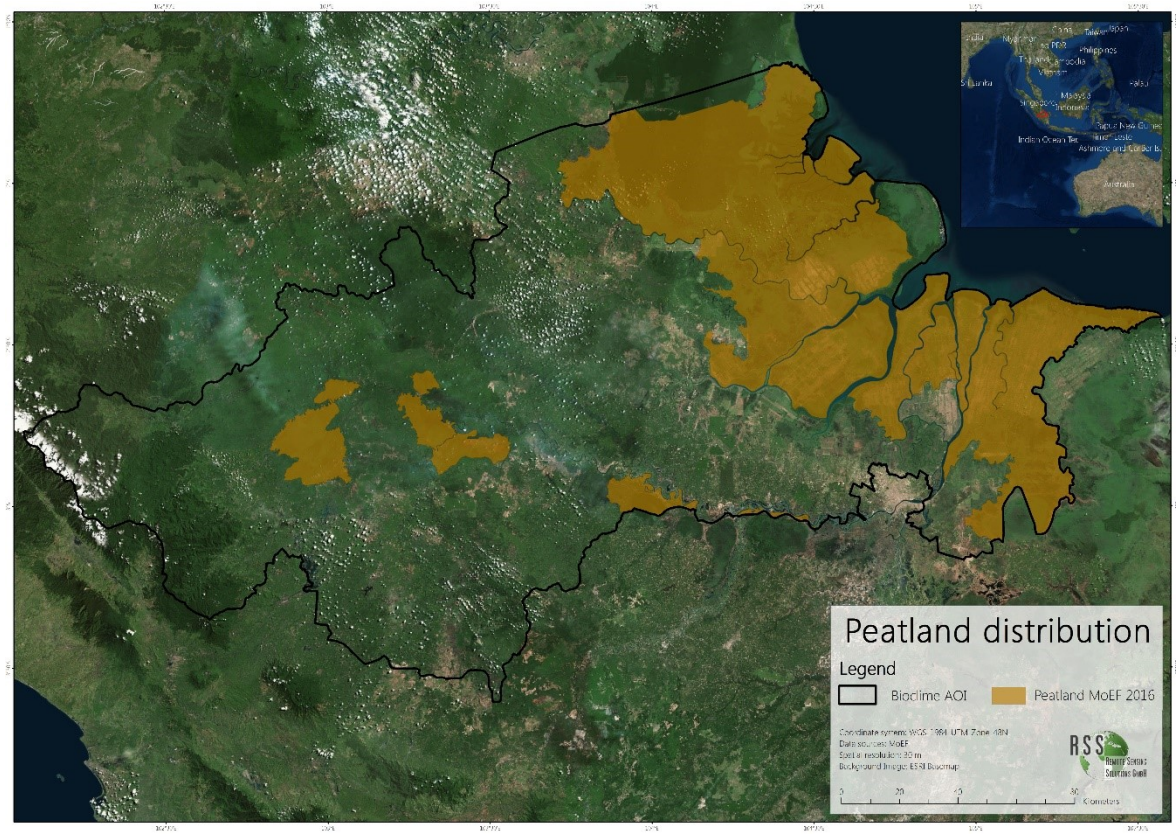

Figure 10: The peatland distribution within the BIOCLIME study area. Derived from the peatland distribution map for 2016 created by the Ministry of Environment and forestry (MoEF).

Burned areas within formerly forested peatlands are considered to be first-fires and therefore a burn depth of 17 cm is applied (see Konecny *et al.* 2016). All other land cover classes are then assigned to second or more fires with a reduced burn depth. So we only discriminate two different stages of fires (first and second or more).

In addition, as we only have the land cover for 1990, 2000, 2005, 2010, 2014 and 2015, we assumed an AGB value of 0 for an area which has been burned twice within one-time window (e.g. 1998 and already burned in 1997), so no emissions from aboveground biomass burning from the second fire. For the peat emissions in such a case this would be classified as second or more fires. Finally, the aboveground emissions and the peat emissions are summed up to get a total number of emissions for the BIOCLIME project area for the designated years. These results are spatially explicit. This allows to exactly determine regions with higher and lower emissions.

3. Results

3.1 Burned area

Burned area maps for 9 different years (1997, 1999, 2002, 2004, 2006, 2009, 2011, 2012 and 2014) were generated (see Figure *11*: Burned area map for the year 1997.Figure 11 to Figure 19). In addition, a burned area map for 2015 based on Sentinel-1 RADAR data was provided from the ESA (European Space Agency) funded Fire CCI (Climate Change Initiative) project, and was integrated into the analysis and results (see Figure 20).

Based on these maps a fire frequency map (a compilation of the single year classifications) was derived (see Figure 21).

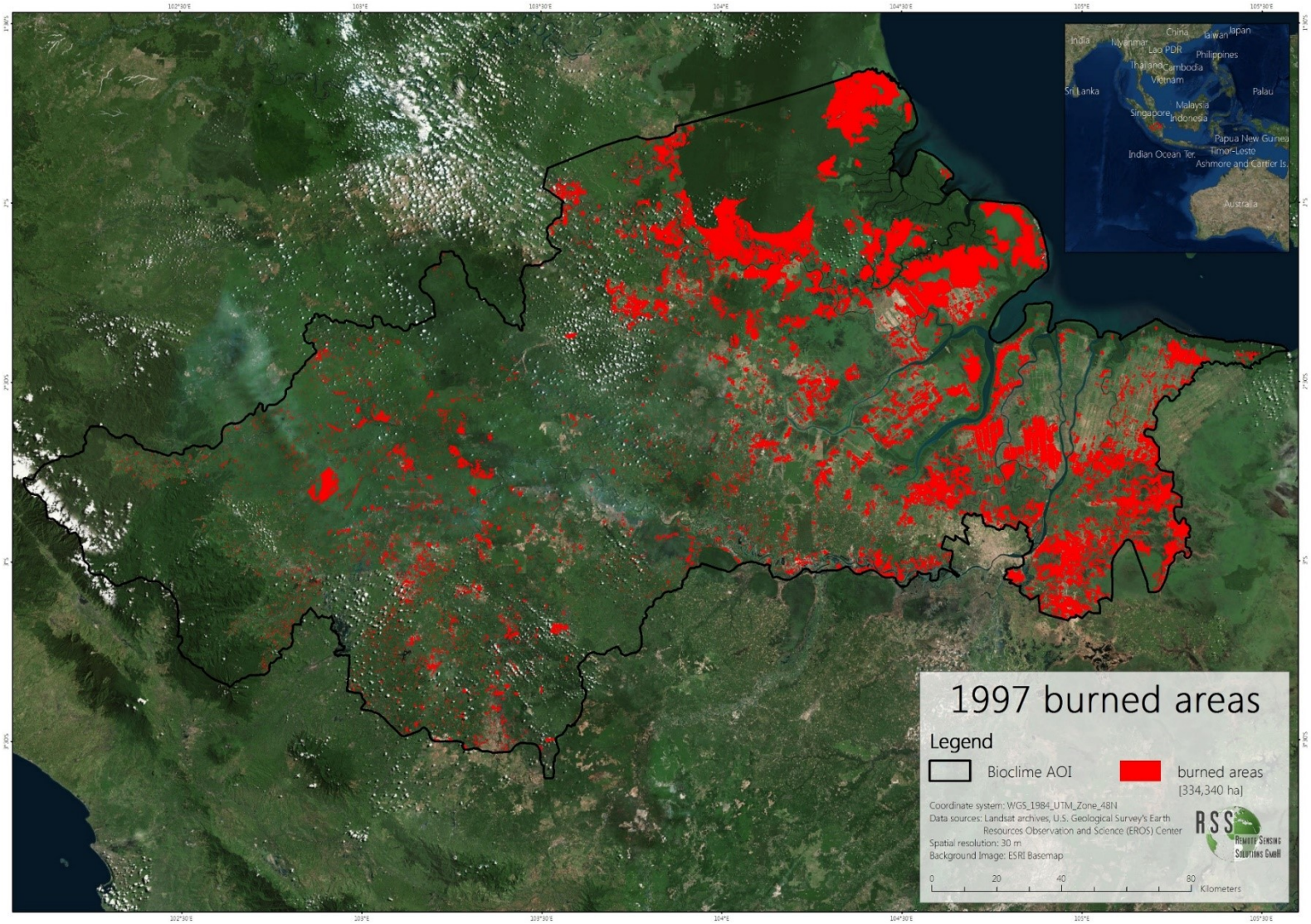

Figure 11: Burned area map for the year 1997.

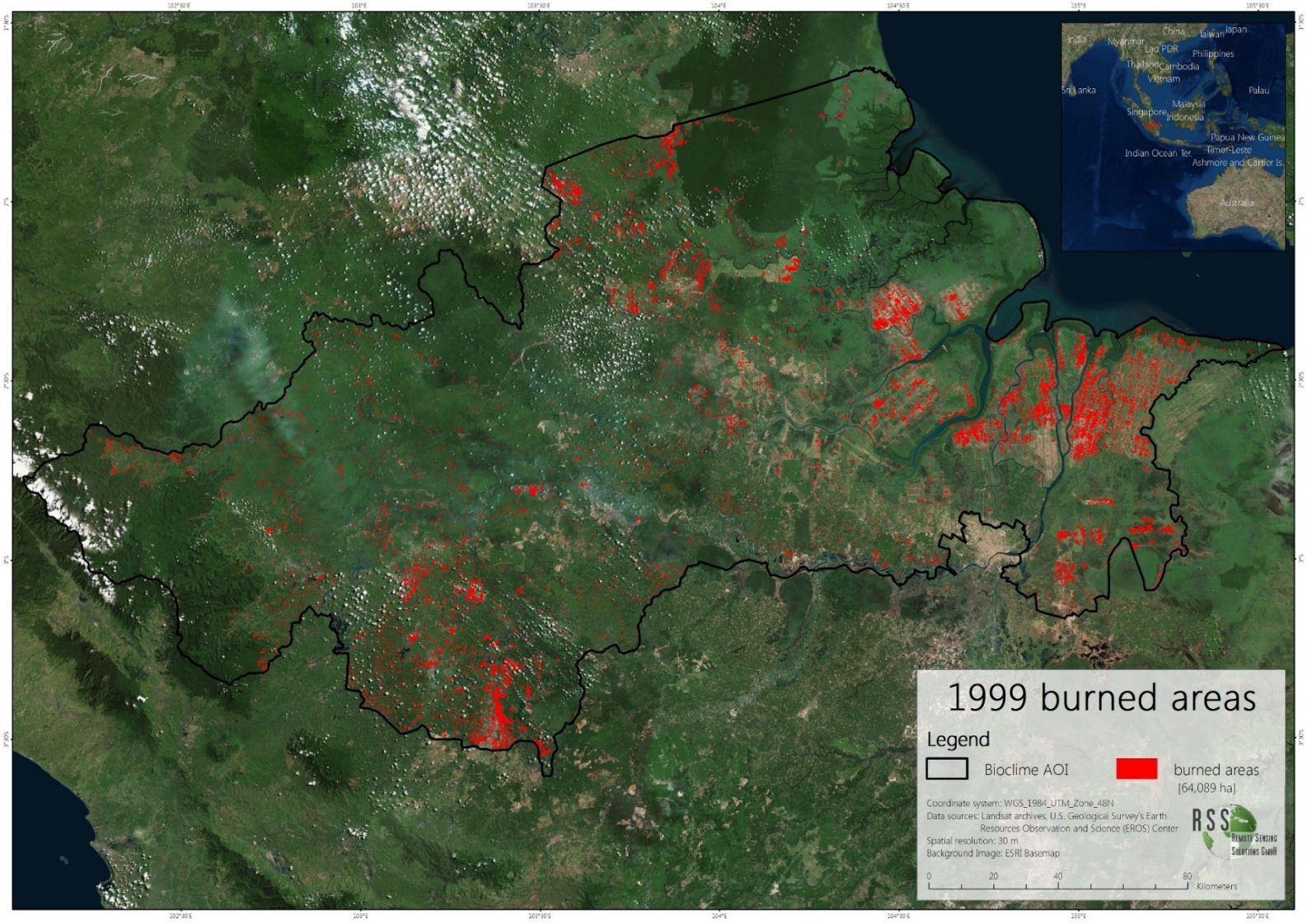

Figure 12: Burned area map for the year 1999.

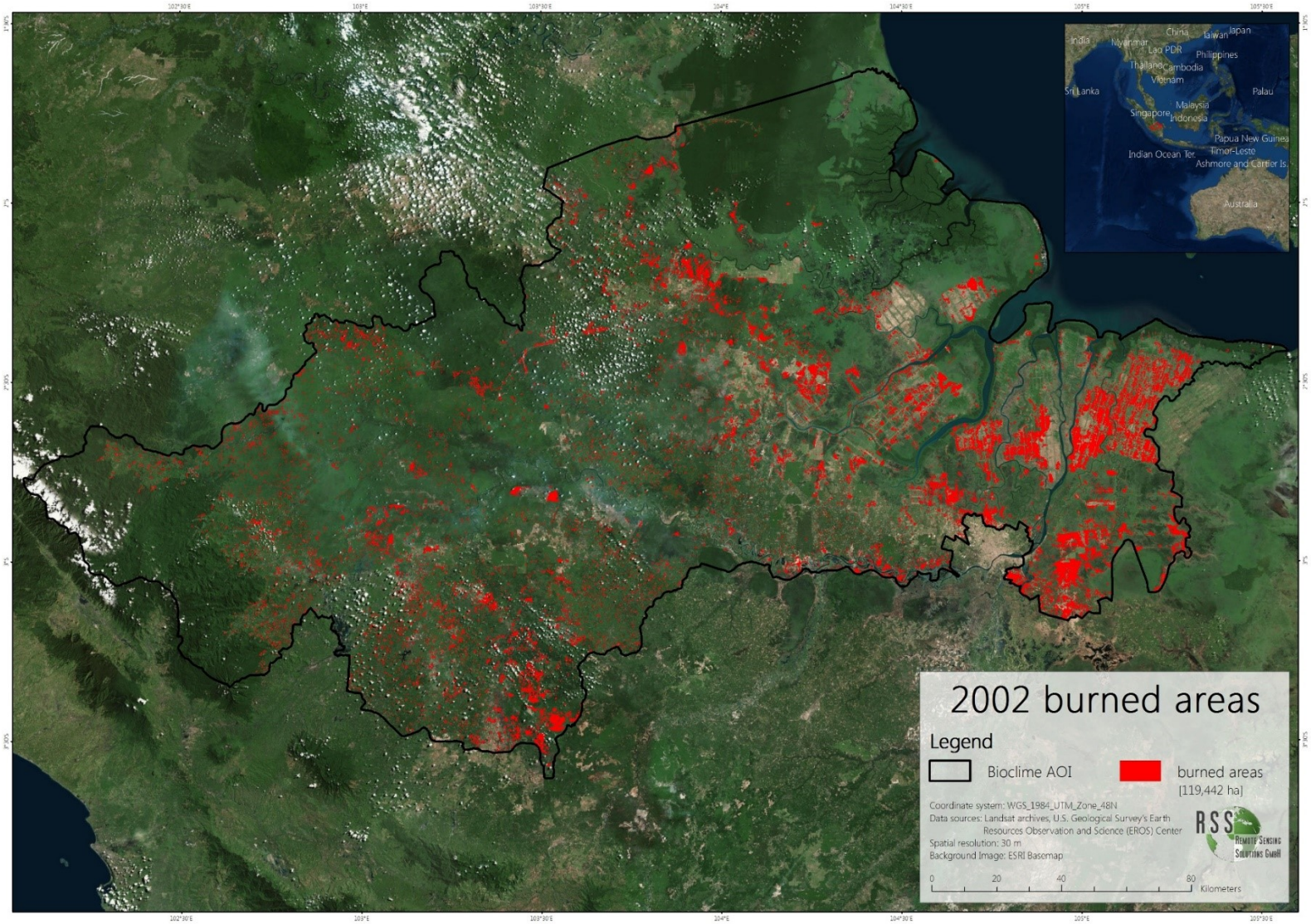

Figure 13: Burned area map for the year 2002.

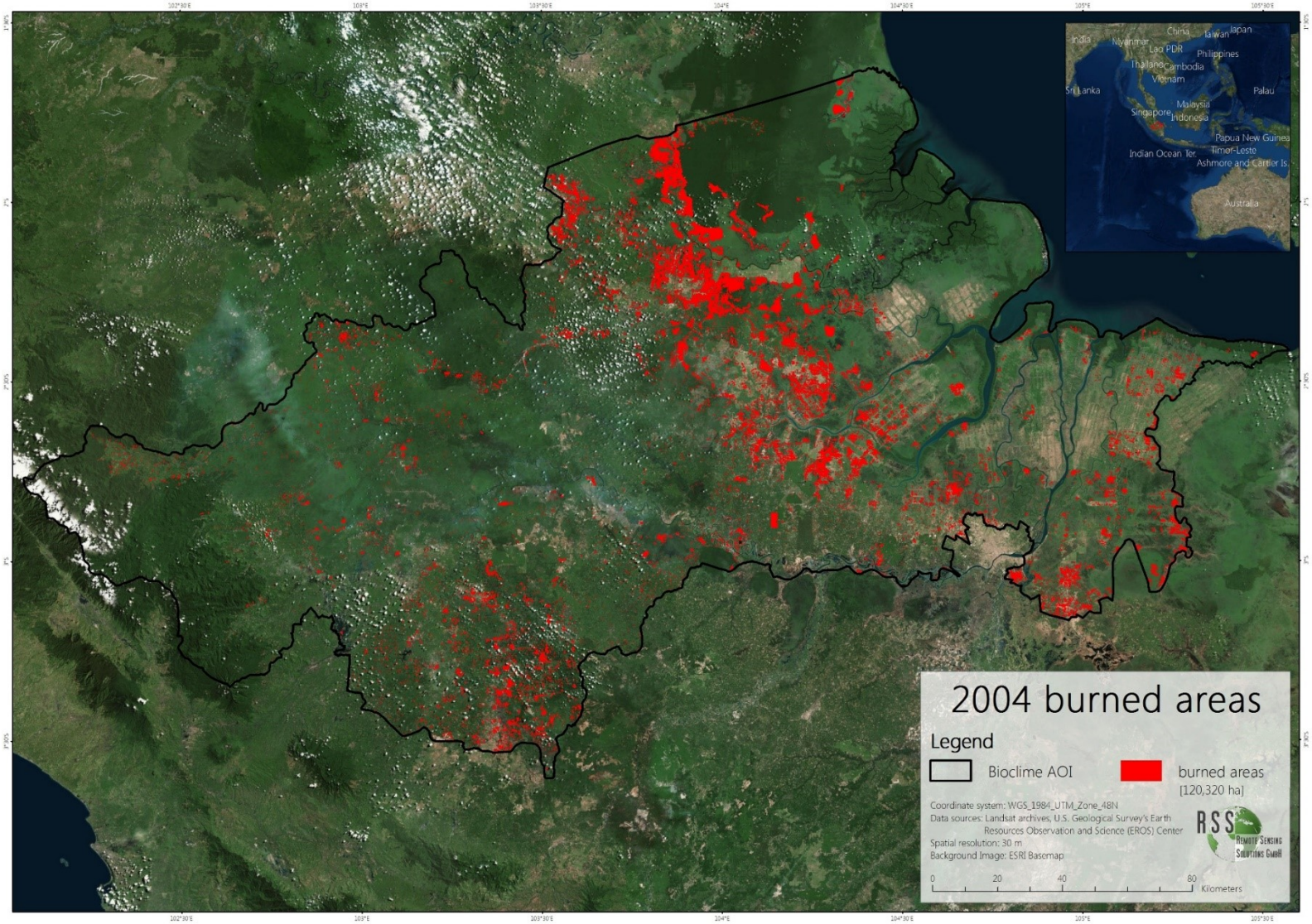

Figure 14: Burned area map for the year 2004.

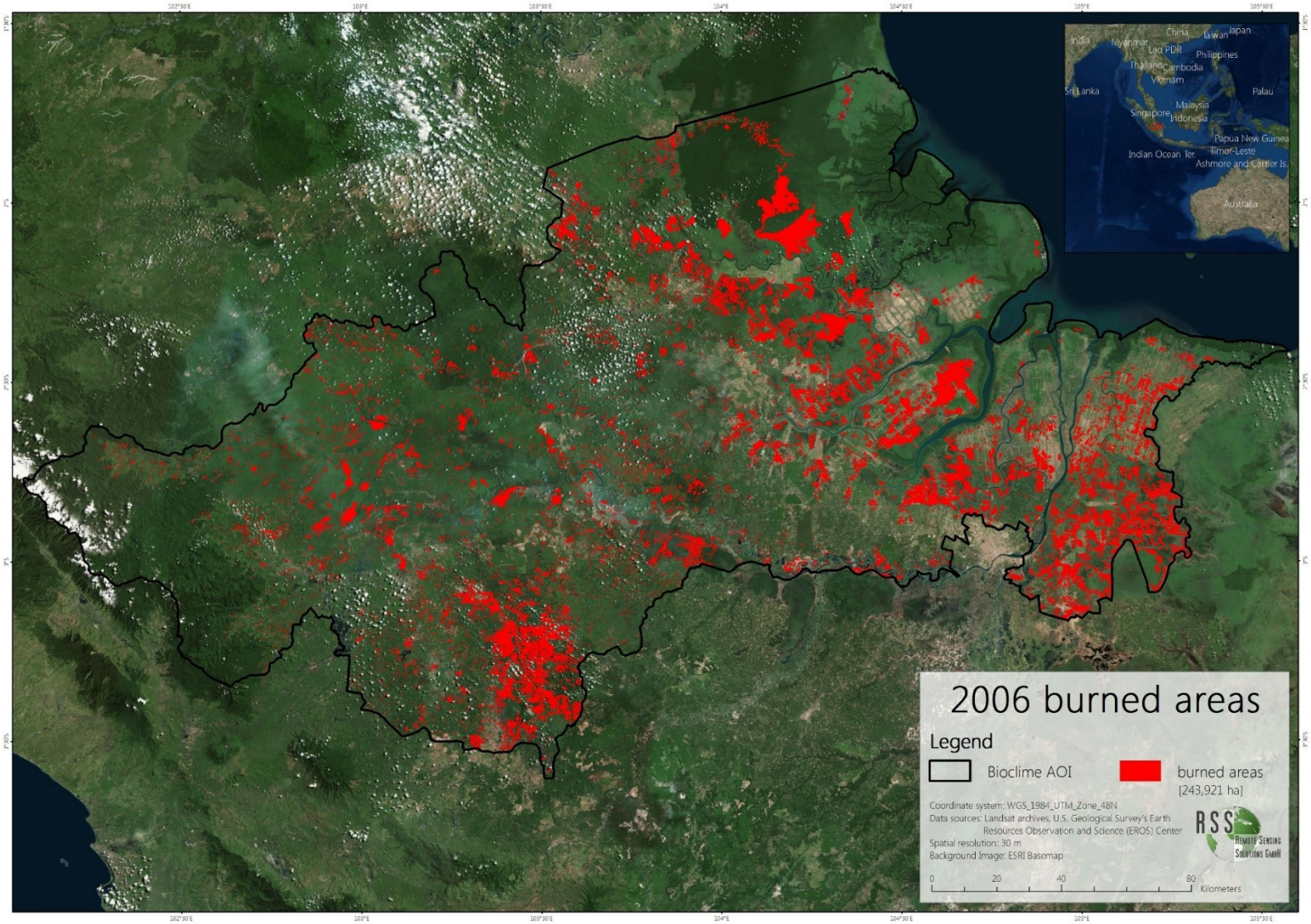

Figure 15: Burned area map for the year 2006.

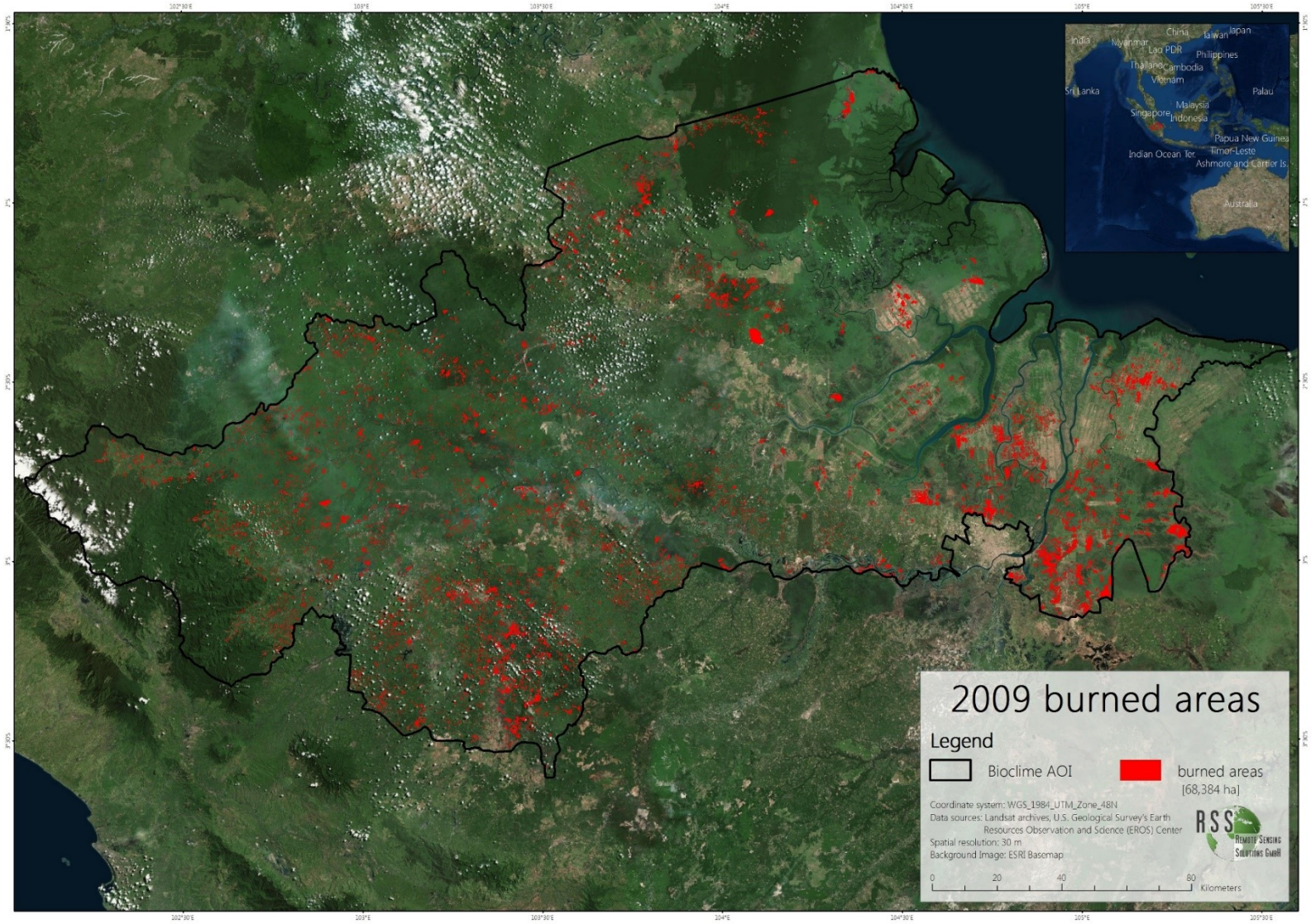

Figure 16: Burned area map for the year 2009.

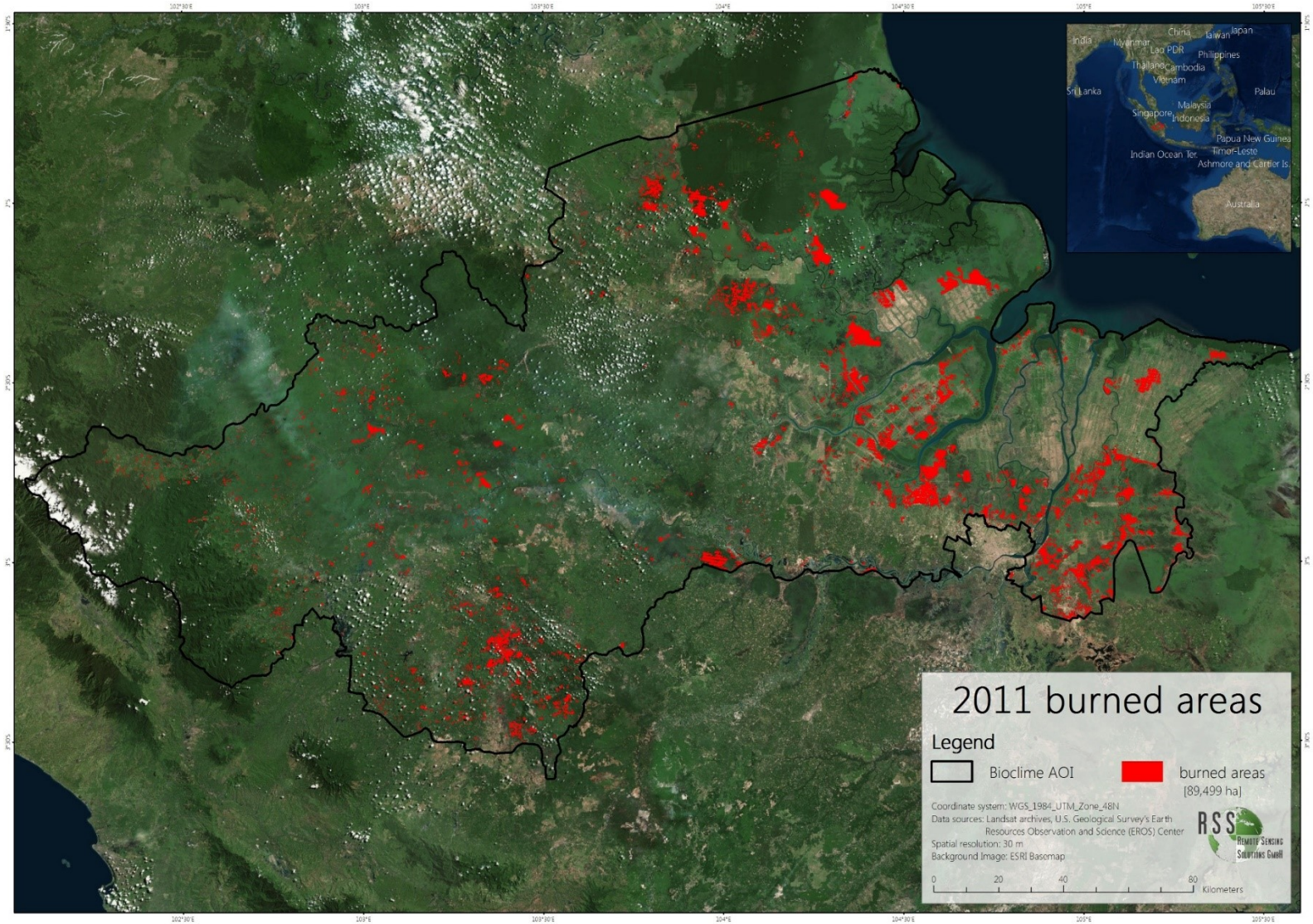

Figure 17: Burned area map for the year 2011.

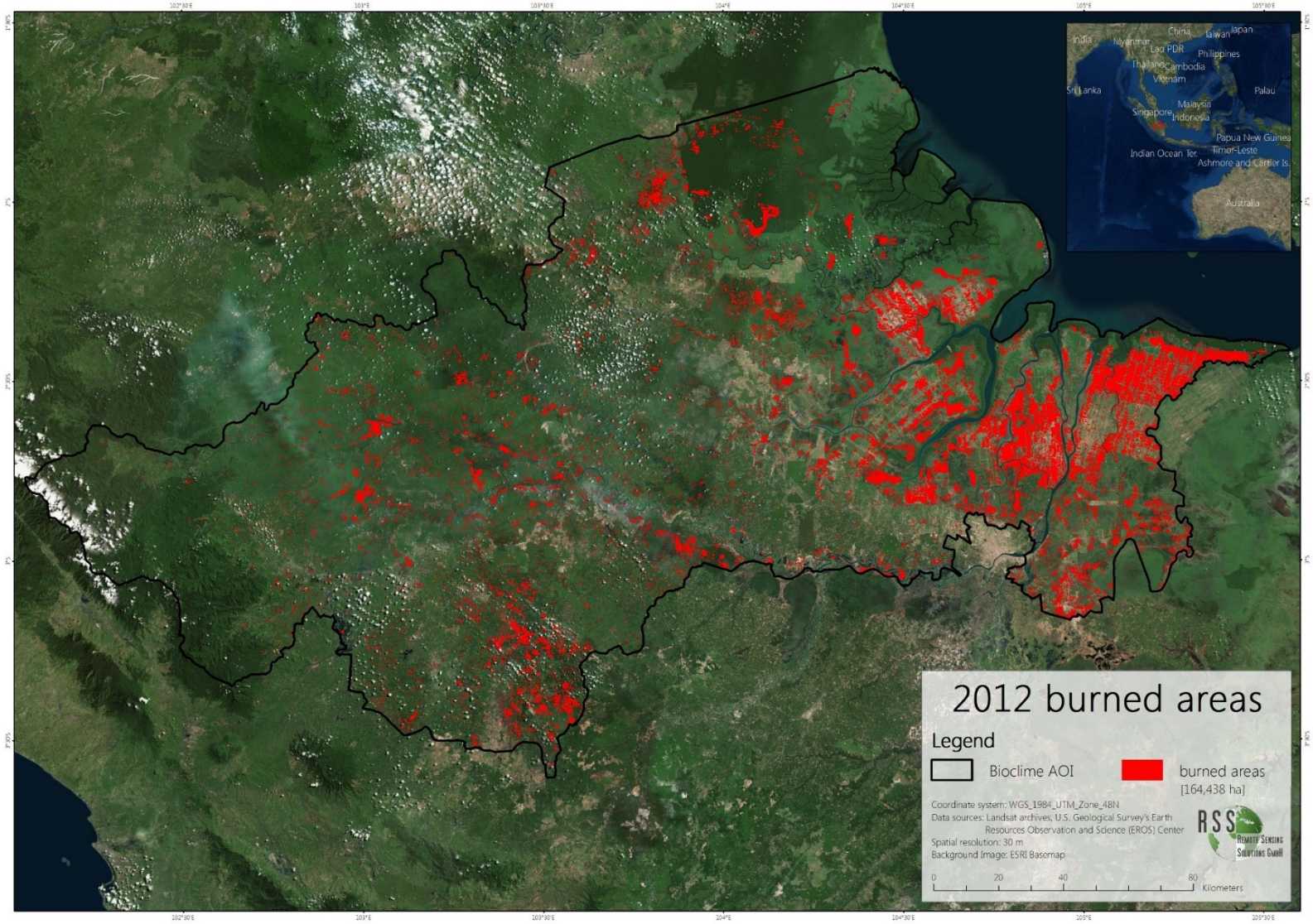

Figure 18: Burned area map for the year 2012.

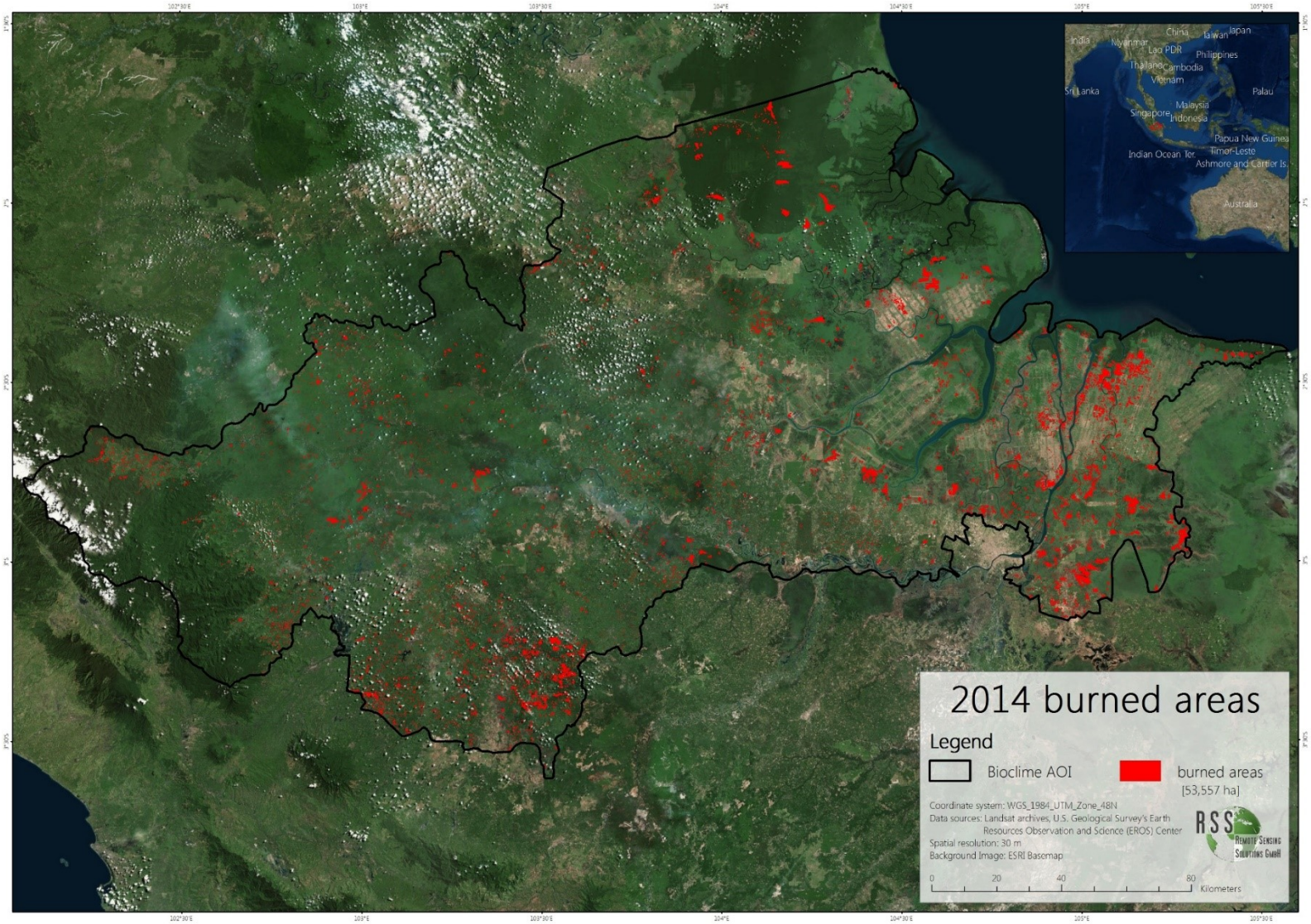

Figure 19: Burned area map for the year 2014.

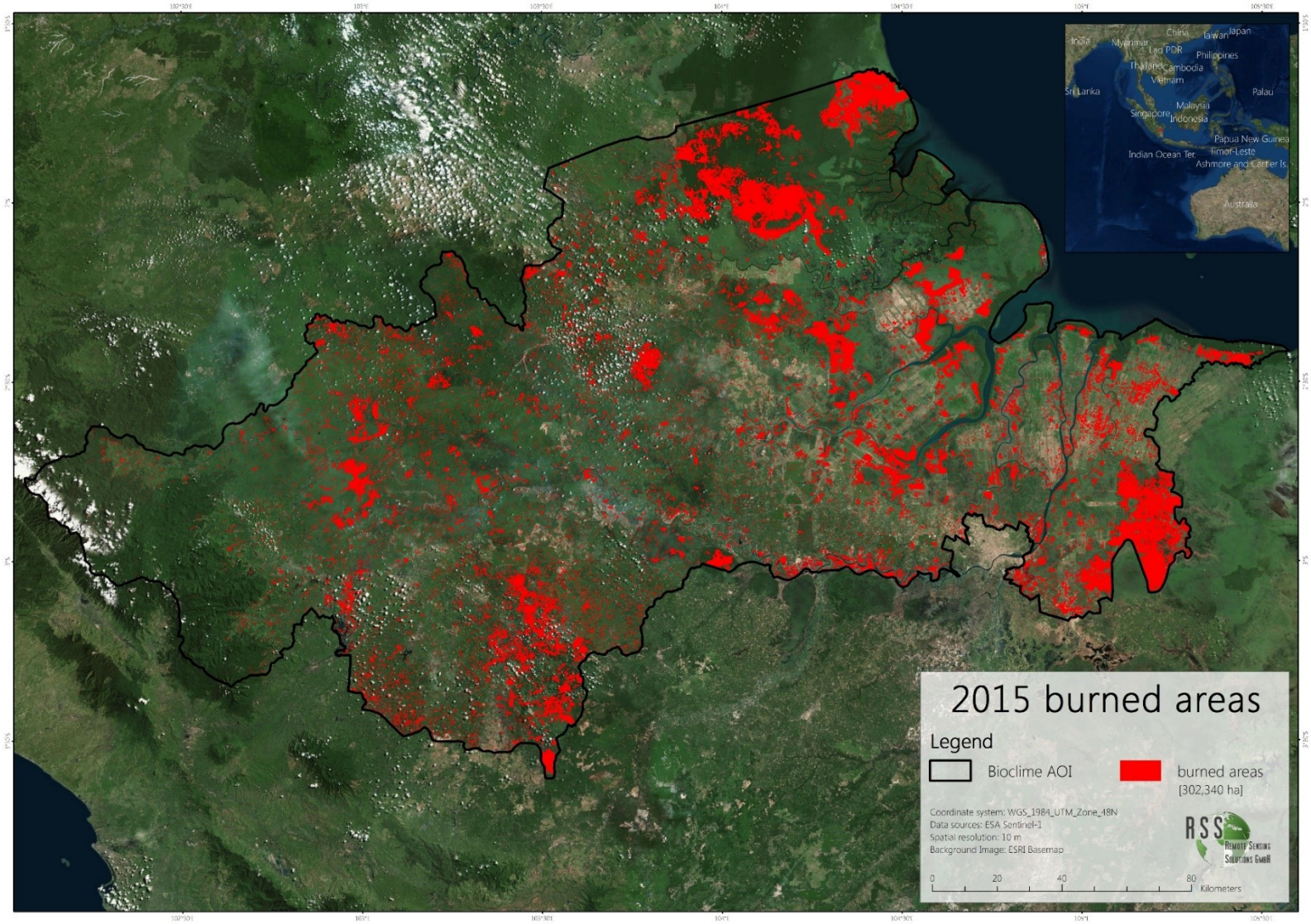

Figure 20: Burned area map for the year 2015 based on Sentinel-1 data (CCI Fire Project).

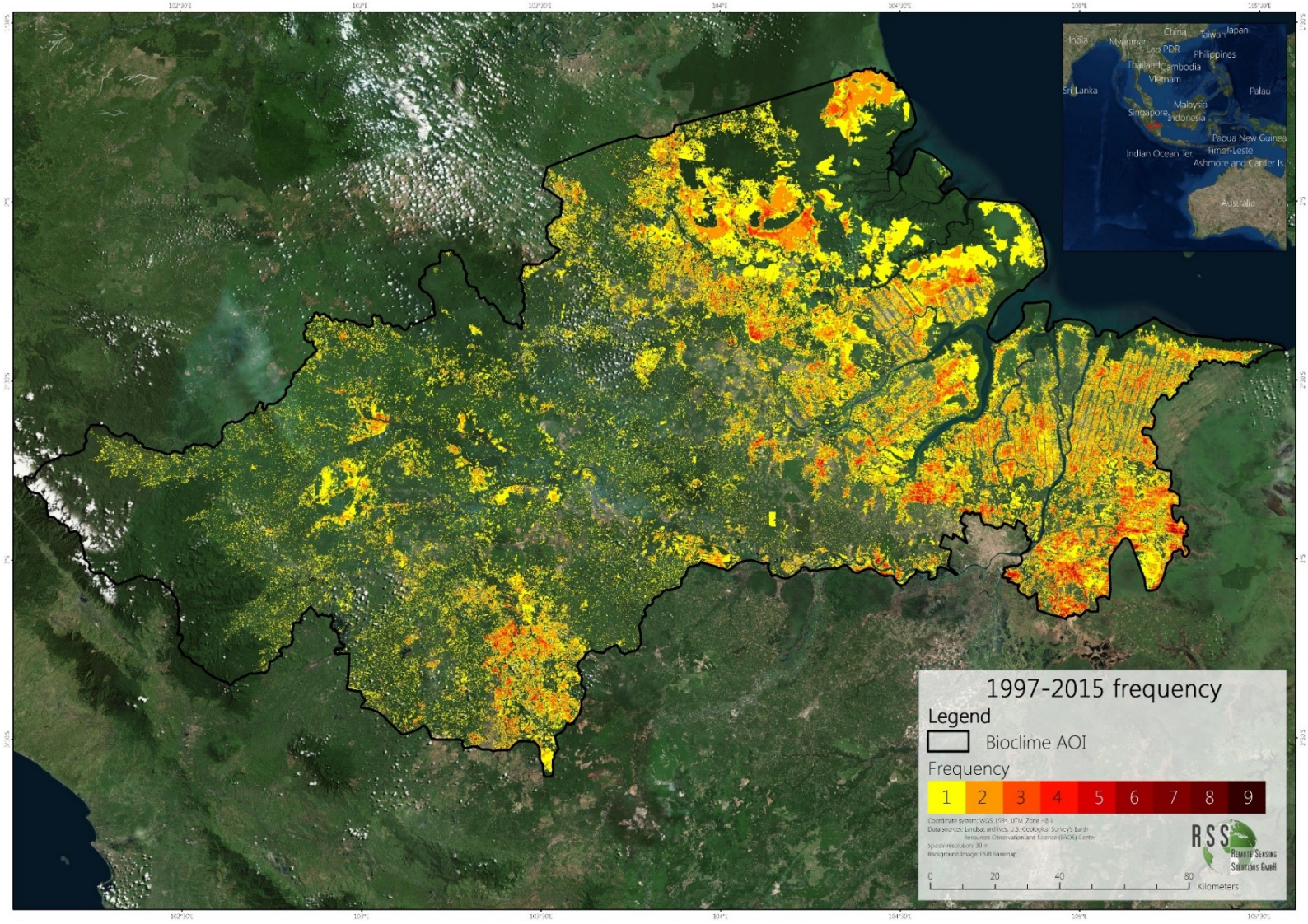

Figure 21: Fire frequency map combining the burned areas of the years 1997, 1999, 2002, 2004, 2006, 2009, 2011, 2012, 2014 and 2015.

Table 4 shows the number of satellite scenes used, the amount of hotspots detected and the total area burned for each year. For the years 1997 (333,931 ha) and 2015 (323,397 ha), by far, the most area burned was detected, with 1997 even higher than 2015.

Table 4: Statistical information about the classified years. Shown are the number of satellite scenes used, the amount of hotspots detected and the total area burned for each year.

Year	No. Scenes	Hotspots	Total Area Burned [ha]
1997	18	16,573	333,931
1999	30	1,888	64,009
2002	37	2,216	119,204
2004	46	2,515	120,029
2006	46	5,494	243,560
2009	57	1,875	68,172
2011	40	2,592	89,310
2012	29	3,319	164,246
2014	41	1,755	53,440
2015	Sentinel-1	8,582	323,397

Figure 22 and Figure 23 display a comparisons between the yearly burned area classified and the amount of hotspots detected for the years 1997, 1999, 2002, 2004, 2006, 2009, 2011, 2012, 2014 and 2015. From these figures it is visible that there is a general trend, but no definite correlation between the amount of hotspots detected and the area burned, so that a direct deduction of burned area from hotspots should always be treated with caution. For example for the years 2004 and 2011 similar amounts of hotspots were detected but in 2004 much more area burned than in 2011 (see also Table 4).

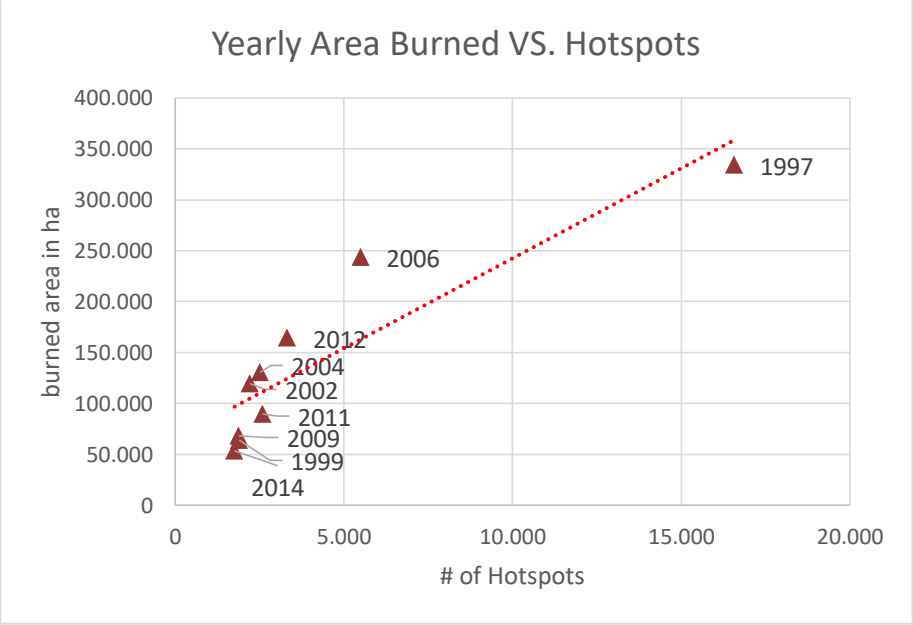

Figure 22: Graph depicting the number of MODIS Hotspots detected during the selected years within the BIOCLIME study area and the mapped burned area for each year in hectares.

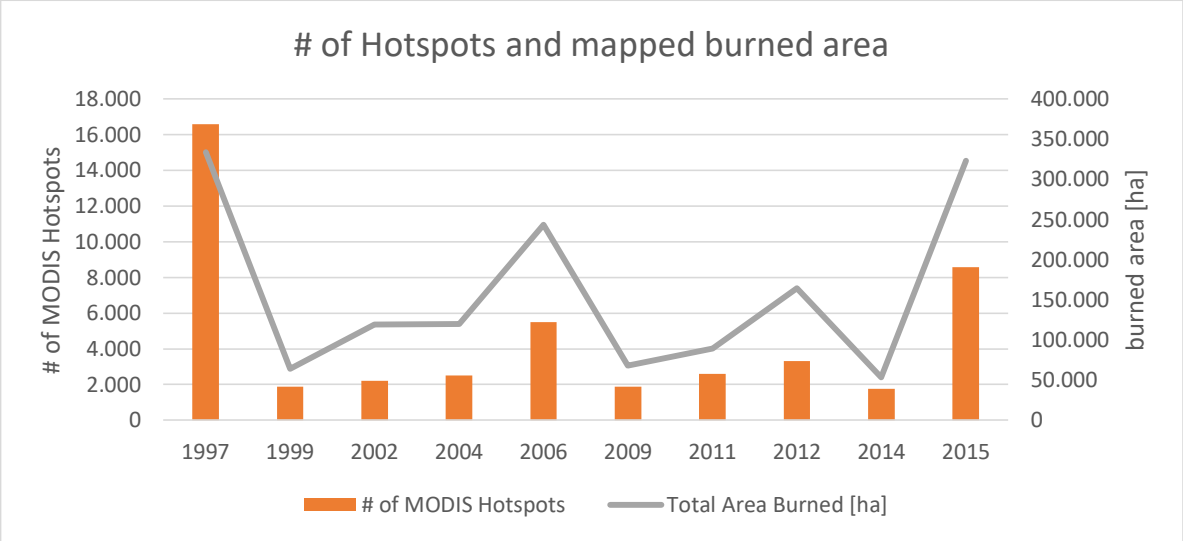

Figure 23: Graph depicting the number of MODIS Hotspots detected during the selected years within the BIOCLIME study area and the mapped burned area for each year in hectares.

3.2 Pre-fire vegetation

Figure 24 depicts the area burned per land cover class for each year.

In 1997 the share of burned primary forest is by far the biggest compared to the other years. 165,865 ha of "Primary swamp forest", 17,710 ha of "Primary dry land forest" and also 3,282 ha of "Primary mangrove forest" burned in 1997. In total this sums up to 186,857 ha of burned primary forest in 1997. The second largest primary forest burning in the BIOCLIME project area took place in 2006 with only (compared to 1997) 17,133 ha of burned primary forest in total. The burning of the land cover class "Tree crop plantation" is increasing over the years and in 2015 more than 106,773 ha of it burned. The same increase over time is visible for the class "plantation forest" where more than 29,275 ha burned in 2015. There is a clear change in ratio of land cover classes burned over the last two decades.

Appendix A gives a detailed overview of the burned area per land cover class and year.

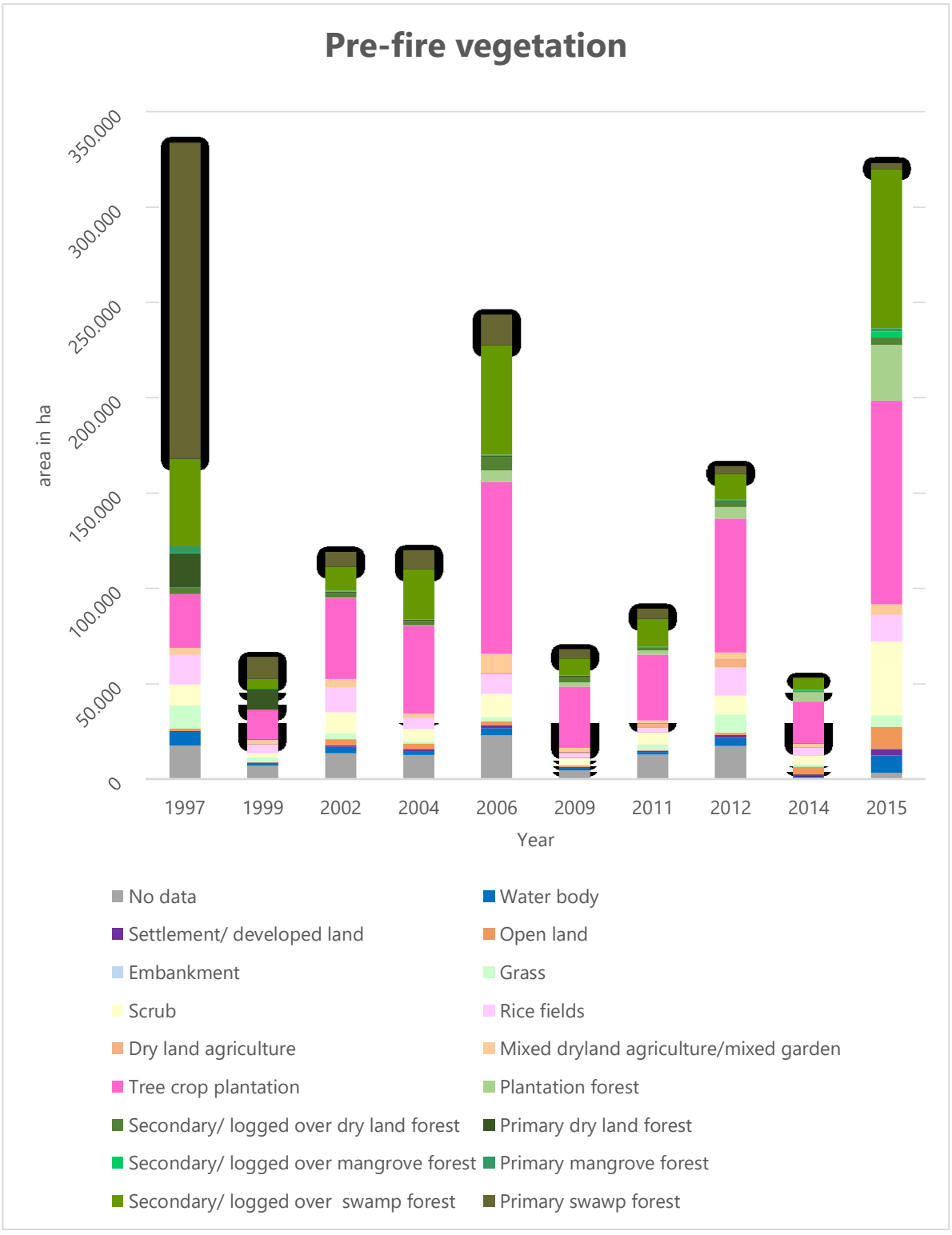

Figure 24: This graph depicts which land cover has burned to which extend within the different years.

3.3 Emissions

Table 5 depicts the aboveground carbon emissions for each mapped year, as well as the peat emissions and the total emissions in megatons of carbon (Mt C). The highest emissions were calculated for 1997 with 46.71 Mt C followed by 2015 with 21.42 Mt C, 2006 with 16.07 Mt C and 2012 with 8.05 Mt C. Further it is visible that emissions are not directly connected to the total burned area. This is also shown in Figure 25, where the X-Axis depicts the years, the Y-Axis the burned area in hectares and the diameter of the circles the amount of carbon emissions. It can be concluded that different land covers lead to different emissions, further the distribution of the peat layer also plays an important role in the amount of emissions.

Table 5: Emissions per year megatons of carbon (Mt C), split up into aboveground (above) and peat emissions.

Year	Area burned (ha)	Emissions (Mt C)		
		Above	Peat	Total
1997	333,931	26.99	20.36	47.35
1999	64,009	3.87	2.01	5.88
2002	119,204	3.02	2.96	5.98
2004	120,029	3.18	3.17	6.35
2006	243,561	7.41	9.45	16.86
2009	68,172	1.84	1.49	3.33
2011	89,310	2.19	3.64	5.83
2012	164,246	2.92	5.70	8.62
2014	53,440	1.03	1.67	2.70
2015	323,397	7.15	14.26	21.42
Total	**1,579,297**	**59.60**	**64.71**	**124.31**

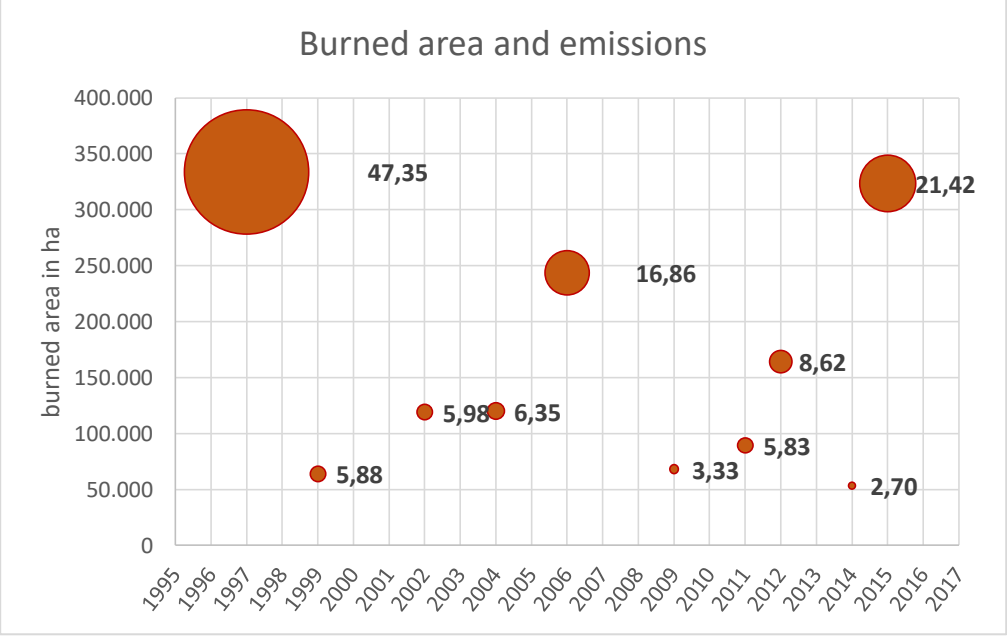

Figure 25: The burned area in ha (Y-axis) for each mapped year (X-axis). The diameter of each circle depicts the emissions in megatons of carbon (Mt C).

Figure 26 Displays the total emissions divided into aboveground and peat emissions in megatons of carbon (Mt C). this figure shows that the ratio of emissions from aboveground biomass to peat changes over time. In the past proportionally more emissions were from aboveground biomass burning whereas in recent years proportionally more emission from peat burning.

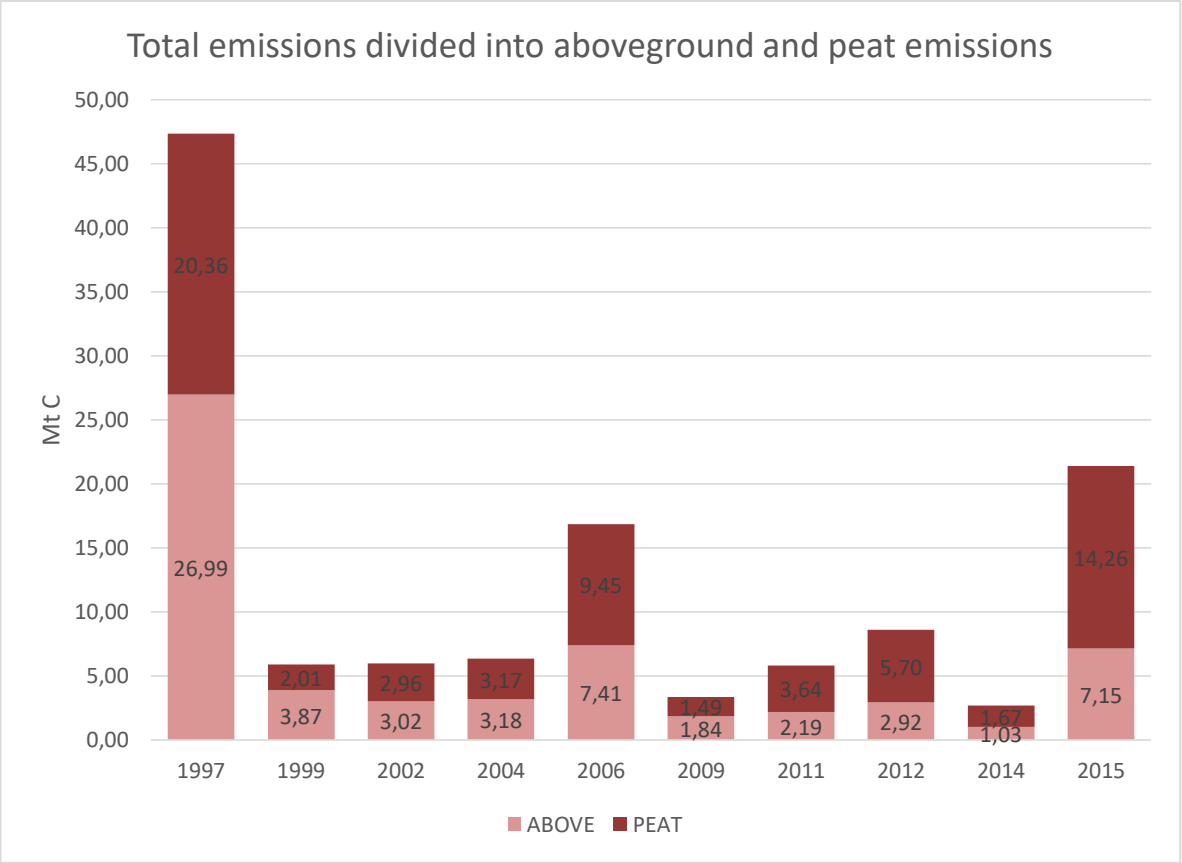

Figure 26: Total emissions divided into aboveground and peat emissions in megatons of carbon (Mt C). The light red bars depict the carbon emissions of the aboveground biomass (ABOVE) and the dark red bars the peat emissions (PEAT).

Table 6 depicts the fraction of burned area within the land cover class “No data”. For these areas emissions were set to zero and therefore have an impact on the total emissions per year. This should be taken into consideration regarding the assessment of the emissions, because no aboveground emissions could be calculated for these areas. If the class “No data” occurred on peat, the value for second or more fires was applied.

Table 6: The burned area per year within the land cover class "No data".

Year	Area burned (ha)	No data (ha)	Percentage
1997	333,931	17,646	5.28%
1999	64,009	7,090	11.08%
2002	119,204	13,591	11.40%
2004	120,029	12,538	10.45%
2006	243,560	22,904	9.40%
2009	68,172	4,782	7.02%
2011	89,310	12,778	14.31%
2012	164,245	17,402	10.59%
2014	53,440	514	0.96%
2015	323,397	3,244	1.00%
Total	**1,579,297**	**112,489**	**7.12%**

4. Conclusions

Following conclusions could be drawn (separated into burned area, carbon emissions from fires and ratio between carbon emission from aboveground biomass and peat burning).

Burned area

- A direct deduction of burned area from the amount of fire hotspots should always be treated with caution (only general trend).
- In 1997 the share of burned Primary Forest is by far the biggest.
- The second largest Primary Forest burning took place in 2006.
- The burning of the land cover classes Tree Crop Plantation and Plantation Forest is increasing over the years.
- There is a clear change in ratio of land cover classes burned over the last two decades.

Carbon emission from fires

- The years with the highest carbon emissions (megatons of carbon Mt C) from fire were:
  - 1997 with 46.71 Mt C (megatons of carbon)
  - 2015 with 21.42 Mt C
  - 2006 with 16.07 Mt C
  - 2012 with 8.05 Mt C
- Emissions are not directly connected to the total burned area.
- Different land covers lead to different emissions, further the distribution of the peat layer also plays an important role in the amount of emissions.

Ration between carbon emissions from aboveground biomass and peat burning

- The ration of emissions from aboveground biomass to peat burning changes over time.
- In the past proportionally more emissions from aboveground biomass burning.
- In recent years proportionally more emissions from peat burning.

5. Outlook

A next step would be to harmonize results from the carbon plots (Work Package 3). As the aboveground biomass calculations derived by the experts from the Bogor Agricultural University (IPB) are based on more differentiated allometric equations (e.g. species specific) it is recommended to use these aboveground biomass estimates to calibrate the LiDAR based aboveground biomass model in Work Package 3, which would lead to revised local aboveground biomass values for the different vegetation classes. This consequently would lead to a recalculation of the aboveground fire emissions (also for Work Packages 1 and 2).

Outputs / deliverables

- Vector data of fire frequency combining the burned areas of the years 1997, 1999, 2002, 2004, 2006, 2009, 2011, 2012, 2014 and 2015 (.shp format)
- Statistics on burned areas and emissions (tables in final report)
- Final report (.docx format)

References

Atkinson P., Lewis P. (2000). Geostatistical classification for remote sensing: an introduction. Comput. Geosci. 26, 361–371.

Baier S.R (2014). Brandflächenklassifizierung in Riau, Sumatra unter Verwendung mittelauflösender Fernerkundungsdaten. Master Thesis, Paris Lodron-University Salzburg.

Guindon B. (2000). Combining Diverse Spectral, Spatial and Contextual Attributes in Segment-Based Image Classification. ASPRS 2000 Annu. Conf. 1–5.

Guindon B. (1997). Computer-Based Aerial Image Understanding: A Review and Assessment of its Application to Planimetric Information Extraction from Very High Resolution Satellite Images. Can. J. Remote Sens. 23, 38–47.

Haralick R., Joo H. (1986). A Context Classifier. IEEE Trans. Geosci. Remote Sens. GE-24, 997–1007.

Hay G.J., Niemann K.O., McLean G.F. (1996). An object-specific image-texture analysis of H-resolution forest imagery. Remote Sens. Environ. 55, 108–122.

Kartikeyan B., Majumder K.L., Dasgupta A.R. (1995). An expert system for land cover classification. IEEE Trans. Geosci. Remote Sens. 33, 58–66.

Kartikeyan B., Sarkar A., Majumder K.L. (1998). A segmentation approach to classification of remote sensing imagery. Int. J. Remote Sens. 19, 1695–1709.

Kettig R., Landgrebe D. (1976). Classification of Multispectral Image Data by Extraction and Classification of Homogeneous Objects. IEEE Trans. Geosci. Electron. 14, 19–26.

Konecny K., Ballhorn U., Navratil P., Jubanski J., Page S.E., Tansey K., Hooijer A., Vernimmen R., Siegert F. (2016). Variable carbon losses from recurrent fires in drained tropical peatlands. Glob Change Biol, 22: 1469–1480.

Matsuyama T. (1987). Knowledge-Based Aerial Image Understanding Systems and Expert Systems for Image Processing. IEEE Trans. Geosci. Remote Sens. GE-25, 305–316.

Melchiori A.E., Setzer A., Morelli F., Libonati R., Cândido P.A., de Jesús S.C. (2014). A Landsat-TM/OLI algorithm for burned areas in the Brazilian Cerrado – preliminary results. VII International Conference on Forest Fire Research D.X. Viegas (Ed.).

Richter R., Schläper D. (2014). Atmospheric / Topographic Correction for Satellite Imagery. 1–238.

Woodcock C.E., Strahler A.H., Jupp D.L.B. (1988). The use of variograms in remote sensing: I. Scene models and simulated images. Remote Sens. Environ. 25, 323–348.

Appendix A

Burned area per land cover class (ICRAF 1990) and year (1997 and 1999).

	ICRAF 1990			
	1997	1999		
BAPLAN LCC (translated from ICRAF)	area [ha]	area [ha]	Burned already 1997 [ha]	burned area [ha]
Tree crop plantation	28,158	15,564	1,478	14,086
Dry land agriculture	320	63	13	51
Embankment	0	0	0	0
Grass	12,119	2,621	733	1,889
Mixed dryland agriculture/mixed garden	3,298	2,498	451	2,047
No data	17,646	7,090	905	6,185
Open land	1,436	155	61	95
Plantation forest	0	0	0	0
Primary dry land forest	17,710	9,924	1,565	8,359
Primary mangrove forest	3,282	195	36	159
Primary swamp forest	165,865	11,503	2,943	8,559
Rice fields	15,702	4,609	1,203	3,406
Scrub	10,920	2,103	599	1,504
Secondary/ logged over swamp forest	46,056	5,220	1,600	3,621
Secondary/ logged over dry land forest	3,596	860	79	781
Secondary/ logged over mangrove forest	408	32	3	29
Settlement/ developed land	412	100	28	72
Water body	7,002	1,471	257	1,214
Sum	333,931	64,009	11,951	52,059

Burned area per land cover class (ICRAF 2000) and year (2002 and 2004).

	ICRAF 2000			
	2002	2004		
BAPLAN LCC (translated from ICRAF)	area [ha]	area [ha]	Burned already 2002 [ha]	burned area [ha]
Tree crop plantation	42,482	45,962	5,275	40,687
Dry land agriculture	128	94	8	86
Embankment	5	25	2	23
Grass	3,022	1,109	283	826
Mixed dryland agriculture/mixed garden	4,135	2,295	342	1,953
No data	13,591	12,538	1,242	11,296
Open land	3,154	2,923	747	2,176
Plantation forest	248	314	7	307
Primary dry land forest	765	704	10	694
Primary mangrove forest	366	170	26	144
Primary swamp forest	7,867	9,933	1,288	8,645
Rice fields	13,106	5,812	1,770	4,041
Scrub	11,071	6,376	1,521	4,855
Secondary/ logged over swamp forest	12,574	26,191	2,596	23,595
Secondary/ logged over dry land forest	2,296	2,157	54	2,102
Secondary/ logged over mangrove forest	191	184	15	169
Settlement/ developed land	986	1,029	278	751
Water body	3,217	2,212	314	1,898
Sum	119,204	120,029	15,779	104,250

Burned area per land cover class (ICRAF 2005) and year (2006 and 2009).

	ICRAF 2005			
	2006	2009		
BAPLAN LCC (translated from ICRAF)	area [ha]	area [ha]	Burned already 2006 [ha]	burned area [ha]
Tree crop plantation	90,159	31,863	5,692	26,171
Dry land agriculture	1,198	309	46	263
Embankment	1	0	0	0
Grass	2,177	550	138	412
Mixed dryland agriculture/mixed garden	9,634	2,531	546	1,986
No data	22,931	4,787	929	3,859
Open land	2,112	738	138	600
Plantation forest	6,179	2,155	344	1,811
Primary dry land forest	883	904	8	897
Primary mangrove forest	183	64	44	20
Primary swamp forest	16,068	4,935	1,048	3,887
Rice fields	10,276	2,643	535	2,109
Scrub	12,071	3,595	1,562	2,034
Secondary/ logged over swamp forest	57,358	8,695	2,902	5,793
Secondary/ logged over dry land forest	6,969	2,816	170	2,646
Secondary/ logged over mangrove forest	89	122	8	114
Settlement/ developed land	1,424	381	106	275
Water body	3,849	1,083	240	843
Sum	243,560	68,172	14,455	53,717

Burned area per land cover class (ICRAF 2010) and year (2011 and 2012).

	ICRAF 2010			
	2011	2012		
BAPLAN LCC (translated from ICRAF)	area [ha]	area [ha]	Burned already 2011 [ha]	burned area [ha]
Tree crop plantation	34,422	70,338	5,130	65,208
Dry land agriculture	2,081	4,598	503	4,094
Embankment	8	61	1	60
Grass	3,115	9,728	691	9,037
Mixed dryland agriculture/mixed garden	1,570	3,189	231	2,958
No data	12,778	17,402	1,637	15,765
Open land	370	1,090	111	978
Plantation forest	2,237	5,988	280	5,708
Primary dry land forest	80	52	2	50
Primary mangrove forest	18	108	0	108
Primary swamp forest	5,351	4,362	540	3,821
Rice fields	2,702	14,914	847	14,067
Scrub	6,211	9,717	1,390	8,326
Secondary/ logged over swamp forest	14,513	13,074	1,335	11,739
Secondary/ logged over dry land forest	1,610	3,565	148	3,417
Secondary/ logged over mangrove forest	207	366	20	345
Settlement/ developed land	710	1,572	120	1,453
Water body	1,326	4,123	178	3,946
Sum	89,310	164,245	13,167	151,079

Burned area per land cover class (ICRAF 2014) and year (2014 and 2015).

	ICRAF 2014			
	2014	2015		
BAPLAN LCC (translated from ICRAF)	area [ha]	area [ha]	Burned already 2014 [ha]	burned area [ha]
Tree crop plantation	21,981	106,773	3,373	103,400
Dry land agriculture	20	99	1	97
Embankment	104	415	3	413
Grass	1,375	6,130	155	5,974
Mixed dryland agriculture/mixed garden	1,940	5,351	113	5,238
No data	514	3,244	66	3,178
Open land	4,035	11,638	464	11,174
Plantation forest	4,876	29,276	1,207	28,068
Primary dry land forest	85	87	2	85
Primary mangrove forest	116	1,753	29	1,724
Primary swamp forest	288	2,988	29	2,959
Rice fields	4,413	13,948	695	13,253
Scrub	4,415	38,699	1,352	37,347
Secondary/ logged over swamp forest	6,301	83,646	1,702	81,945
Secondary/ logged over dry land forest	659	3,722	48	3,674
Secondary/ logged over mangrove forest	557	3,081	287	2,794
Settlement/ developed land	728	3,425	83	3,342
Water body	1,030	9,122	180	8,942
Sum	53,440	323,397	9,790	313,607